JIMMA UNIVERSITY

SCHOOL OF GRADUATE STUDIES

DEPARTMENT OF CHEMISTRY

GREEN SYNTHESIS AND CHARACTERIZATION OF MAGNETIC IRON OXIDE NANOPARTICLES CAPPED BY *Maesa lanceolata* L. LEAF EXTRACT AND ITS METHYLENE BLUE DEGRADATION APPLICATION

FEBRUARY, 2021

JIMMA- ETHIOPIA

GREEN SYNTHESIS AND CHARACTERIZATION OF MAGNETIC IRON OXIDE NANOPARTICLES CAPPED BY *Maesa lanceolata* L. LEAF EXTRACT AND ITS METHYLENE BLUE DEGRADATION APPLICATION

A THESIS SUBMITTED TO SCHOOL OF GRADUATE STUDIES JIMMA UNIVERSITY IN PARTIAL FULFILLMENT OF THE REQUIRMENTS FOR THE DEGREE OF MASTERS OF SCIENCE IN INORGANIC CHEMISTRY

BY: ADEME KEKAMO

ADVISOR: GUTA GONFA (Ph.D)

CO-ADVISOR: GEBRU GEBRETSADIK (Ph.D Candidate)

FEBRUARY, 2021

JIMMA- ETHIOPIA

TABLE OF CONTENTS

Contents **Pages**

LIST OF TABLES

Tables **Pages**

LIST OF FIGURES

Figures **Pages**

LIST OF ABBREVIATIONS AND ACRONYMS

FE-SEM	Field-emission scanning electron microscopy
FT-IR	Fourier transforms infrared
MB	Methylene blue
NPs	Nanoparticles
NZVI	Nano zerovalent iron
PPM	Parts per million
PZC	Point of zero charge
PAA	Poly acrylic acid
SEM	Scanning electron microscopy
SPR	Surface Plasmon resonance
TEM	Transfer electron microscopy
UV-Vis	Ultraviolet-visible
VSM	Vibrating sample magnetometer
XRD	X-ray diffraction

ACKNOWLEDGEMENTS

First of all I would like to give the greatest possible glory and thanks to my God, the one responsible for the accomplishment of this thesis.

Next I would like to express my sincere gratitude to my advisors Guta Gonfa (Ph.D) and Gebru Gebretsadik (Ph.D Candidate) for their invaluable guidance, genuine concern to help in any aspect, unreserved support, constant encouragement, sitting for longer hours of discussions and consultations, and comments on the work throughout the work.

I would like to express my very great appreciation to the department of Chemistry and members of the department, Jimma University for giving great opportunity to study my M.Sc in inorganic chemistry and for delivering me laboratory facilities, instrumentation and for assistance in their areas of knowledge which enabled me to complete this research work as well as material engineering department for conducting XRD and FT- IR analysis for my samples.

My special appreciation goes to Tsegaye Girma (Ph.D) for his great effort to make my research work highly meaningful by giving immeasurable comments and advices.

My genuine acknowledgment is also extended to Bonga College of teacher's education office for sponsorship they have given me to pursue my M.Sc study.

I have, however, no words to thank my wife Bizunesh Kebede, who stayed with me in times of failure and in times of success, and in times of happiness and in times of hardships throughout this program.

I have also great appreciation for my class mates Dereje Dadi and Buzunesh Temesgen for their valuable supports.

Finally, I would like to thank all individuals and organizations who have contributions in one or other ways for completion of this work.

ABSTRACT

Disposal of untreated sewage, coloring dyes and release of pollutant gases to the atmosphere due to increase in population number and rapid growth of industrialization, causes water pollution. Water pollution problem is getting very severe all over the world. So, it is very important to search for high performance materials for solving the problem. The main objective of this study was to synthesize, characterize and to investigate photocatalytic dye degradation activity of magnetic iron oxide nanoparticles (Fe_3O_4 NPs). Fe_3O_4 NPs were synthesized *via* green synthesis method by taking ferric chloride hexahydrate ($FeCl_3.6H_2O$) and ferrous chloride tetra hydrate ($FeCl_2.4H_2O$) (2:1 molar ratio) and *Maesa lanceolata* L. leaf extract as capping agent. The synthesized Fe_3O_4 NPs were characterized using UV-Vis spectroscopy, FT-IR spectroscopy and XRD spectroscopy. The UV-Vis spectroscopy shows the characteristic peak of Fe_3O_4 NPs at 370 nm. FT-IR spectroscopic study of the plant extract and the synthesized Fe_3O_4 NPs revealed the formation of Fe_3O_4 NPs by coordination with the functional groups present in the plant extract. The XRD analysis elaborated the formation of crystalline Fe_3O_4 NPs and used to estimate the average crystalline size that is about 14.6 nm. The formation of nanometer sized Fe_3O_4 NPs makes promising candidate for photocatalytic degradation of methylene blue (MB) dye. As a result, the degradation efficiency of Fe_3O_4 NPs on a model organic dye MB after optimization (pH=10, the mass of the Fe_3O_4 NPs=30 mg, concentration of MB=5 mg/L and temperature=60 ºC) was found to be 94.3%. In this study, Fe_3O_4 NPs were successfully synthesized using an aqueous leaf extract of *Maesa lanceolata* L. *via* green route method and the nanocatalysts were highly efficient for methylene blue photocatalytic degradation.

Key words: *Fe_3O_4 nanoparticles, green synthesis, photocatalytic degradation, plant extract*

1. INTRODUCTION

1.1. Background of the study

The increase in population numbers, industrial pollution and changes in climate are the main factors leading to water scarcity and a decrease in the quality of potable water. The problem of water pollution is getting very severe, especially in developing countries like Ethiopia. The widespread presence of organic dyes in industrial wastewaters from the textile, apparel, and paper industries results in significant environmental contamination. These dye-polluted effluents contain highly hazardous, carcinogenic, non-biodegradable, and colored pigments that can cause damage to humans. Most industries use MB for coloring different products like food, soap, sugar, textile products pants and others. However, acute exposure to MB will cause health problems such as, increasing heart rate, vomiting, shock, cyanosis, and tissue necrosis in humans [1, 2]. Even at very low concentrations (below 1 ppm), MB is clearly visible in the water and seriously deteriorate aqueous environments. Water contamination continues to be a major environmental problem worldwide. The United Nations estimates around 3.1% of deaths worldwide, which is over 1.7 million deaths a year, are caused by unsafe or inadequate access to water. Access to clean water is not only a human right, but also a necessary factor for economic productivity and technological development [2].

So, the removal of colored organic dye effluents from wastes is imperative and important. Currently, many developing countries use routine wastewater treatment techniques such as boiling, sedimentation, treatment with chemical disinfectants and traditional cloth filtration methods. But, these methods have several disadvantages like, they cannot remove dissolved salts and some soluble inorganic and organic substances completely, they are very expensive, chemicals have many side effects and they are not eco-friendly. In addition to this, communities in undeveloped rural areas usually have no water purification plants and are prone to develop life-threatening diseases. In many cases, they have to rely on rivers, open reservoirs; springs and open wells for water supply. The lack of proper sanitation facilities exacerbates the problem and wells with water are often located close to dug-out latrines, bathing areas and animal camps [3].

So, it is very important to search for advanced technologies for solving problems related with water contamination. In this context, nanotechnology could help in solving the problems concerning water quality and environmental pollution [4].

Nowadays, nanoparticles (NPs) and their technologies are booming rapidly due to their enormous applications. Nanoparticles (NPs) are particles at least one of their dimensions range 1–100 nm in size.

The large surface area to volume ratio of NPs exhibit enhanced catalytic reactivity, biological activities, thermal conductivity, non-linear optical performance, and chemical steadiness in comparison to their bulk form [4]. As a result of these properties, NPs have wide applications, such as in health, food, feed, space, chemical, cosmetic industries, water treatment and in agriculture.

Numerous chemical and physical methods are used for the synthesis of nanoparticles. However, as a result of the difficulties in scaling up and intense energy requirements in physical processes and the use of toxic chemicals like sodium borohydride as reducing agent, hydrazine and sodium dodecyl sulfate as surfactant that could be carried in chemical processes, alternative methods are required [4-5].

Therefore, there is a paradigm shift toward cheap, sustainable, green and eco-friendly methods, which can be used for the synthesis of nanoparticles. Numerous biological resources such as algae, fungi, bacteria and plants have emerged as cost effective and eco-friendly platforms for the synthesis of nanoparticles. The interface of medicinal plants and biogenic nanoparticles has attracted many researchers to fabricate nanomaterial with diverse applications [5].

The plant mediated synthesis approach is preferable over other biogenic methods due to time wastage, difficulty in incubation period, rich phytochemistry and bioactive components and material cost [6]. Plant mediated methods are more effective for the generation of NPs with the advantage of less chances of failure, low cost, non-toxicity (environmental compatibility) and ease of characterization [1]. The bio molecules such as flavonoids, terpenoids, polyphenols, sugars, alkaloids, phenolic acids, and proteins which are present in the plant materials (leaf, stem, seed and root) can increase the rate of nanoparticle synthesis or the stability of the product. Flavonoids show best capping capacity due to chelate or ring formation since they act as poly dentate ligands [5-6]. Plant mediated synthesis has been employed for the synthesis of metallic and metal oxide NPs with an aim to make use of environmental-friendly reducing and stabilizing agents. Instrumental methods like UV-Vis, FT-IR and XRD are used to characterize the synthesized NPs.

Magnetic iron oxide nanoparticles (Fe_3O_4 NPs) differ from other iron oxide nanoparticles due to the presence of both Fe^{2+} and Fe^{3+} combinations, where divalent ions are organized at the octahedral sites and trivalent ions are split across the tetrahedral and octahedral sites.

However, α-Fe_2O_3 contains Fe^{3+} ions distributed at their octahedral sites and in case of γ-Fe_2O_3 (termed oxidized magnetite), Fe^{3+} cations are distributed in octahedral and tetrahedral sites along with Fe^{2+} cation vacancies located at octahedral sites. Magnetic iron oxide nanoparticles (Fe_3O_4 NPs) are widely used in the field of water contamination remediation [7-12].

Photocatalytic dye degradation processes have advantages for the removal of pollutants even at low concentration for industrial waste water [5]. Essentially, the photocatalytic reaction involves heterogeneous catalysis, where a light-absorbing catalyst is put in contact with the target reactants, in either a solution or gas phase. This heterogeneous approach was successfully employed as an effective tool for the degradation of various hazardous materials (pollutants) and shows many advantages over traditional waste water treatment techniques. In photodegradation, electrons are excited to the conduction band (CB) of the photocatalyst, while holes are formed in the valance band (VB) upon irradiation with incident photons [6]. The photoexcited electrons and holes can either recombine to generate thermal energy or diffuse to the photocatalyst surface reacting with the adsorbed molecules. The reactive radical species, such as superoxide radicals ($\cdot O_2^-$) and hydroxyl radicals (·OH), are further derived from the photoexcited electrons and holes, respectively. Moreover, the photosensitization of dye molecules can provide photocatalyst with additional electrons, which are also capable of generating radicals like O_2^-.

A *Maesa lanceolata* L. called false Assegai (English), Chaggo (Kaffigna), Abayi (Oromiffa), Kelawa (Amharic) is a shrub or small tree about 5 m with simple, wide oval, usually up to 10 cm long, shiny green above, pale below, thick and leathery, the edge well toothed, tip pointed, a leaf stalk 2–3 cm, often yellow leaf. Bioactive compounds such as phenols, terpenoids, anthraquinones, flavonoids, saponins and alkaloids are present on the leaf, roots and stem bark extracts of the plant [13]. In Ethiopia its yellow fruit yield oil which is used to grease new pottery as a waterproofing agent and traditional medicine [11].

In the present study, green synthesis method was employed for the synthesis of magnetic iron oxide (Fe_3O_4) nanoparticles using *Maesa lanceolata* L. leaf extract as a capping agent leading to reduced aggregation and to increase stability of the NPs.

The iron oxide NPs synthesized was characterized by UV-Vis, FT-IR and XRD instruments and their photocatalytic dye degradation application was investigated.

1.2. Statements of the problem

Nanotechnology plays a vital role in solving persistence environmental problems due to industrial dye effluents like methylene blue dye. Different studies have been conducted before, in the area of synthesis of nanomaterials. But most researchers focus on chemical methods that use very expensive as well as hazardous chemicals as reducing, capping and stabilizing agents that cannot be easily degraded. Physical methods are also carried out at high temperatures, which generate a large amount of heat.

Green synthesis is eco-friendly, simple, cost effective, one pot reaction, amenable to scale up, toxicity associated with hazardous chemicals are reduced, biocompatible and biological entities can be used as reducing, capping and stabilizing agents.

In this regard, no study have been carried out on green synthesis of Fe_3O_4 NPs using aqueous extract of *Maesa lanceolata* L. leaf, since using different plant extract as a capping agent results the formation of nanoparticles with different particle size. So that, the current research work mainly focus on green synthesis of Fe_3O_4 NPs using aqueous extract of *Maesa lanceolata* L. leaf as a stabilizing agent, characterization of synthesized Fe_3O_4 NPs and evaluation of their photocatalytic activity.

In this study the following questions were to be answered.

1. Is *Maesa lanceolata* L. leaf extracts an effective stabilizing agent to be used for green synthesis of Fe_3O_4 NPs?
2. Can information obtained from UV-Vis, FT-IR and XRD instruments used to describe the characteristics of the synthesized magnetic iron oxide NPs?
3. Does the synthesized Fe_3O_4 NPs have potential efficiency for photocatalytic degradation of MB?

1.3. Objectives of the study

1.3.1. General Objective

- To investigate the synthesis, characterization and to know the potential dye degradation application of the synthesized Fe_3O_4 NPs *via* green synthesis method using *Maesa lanceolata* L. leaf extract as reducing and stabilizing agent.

1.3.2. Specific objectives

- To synthesize Fe_3O_4 NPs by using *Maesa lanceolata* L. leaf crude extract as a reducing and stabilizing (capping) agent.
- To characterize the synthesized Fe_3O_4 NPs using UV-Vis, FT-IR and XRD instruments.
- To evaluate the photocatalytic dye degradation efficiency of the synthesized Fe_3O_4 NPs using model organic dye MB.

1.4. Significance of the Study

This research study has the following significances:

1. This study obeys one of the objectives of green chemistry which is reduction of hazardous chemicals through alternative route on Fe_3O_4 NPs synthesis and the application of green chemistry principles to the field of nanotechnology. In this regard, this research output may motivate other researchers to study more on this research area.
2. This research material can be used as a reference for other researchers because there was no any reported study up to now on green synthesis of Fe_3O_4 NPs using aqueous extract of *Maesa lanceolata* L. leaf.
3. The application of nanoparticles is relatively effective, efficient, energy saving environmentally benign and cost effective when compared with bulk materials. So that, the output of this study may be scaled up by concerned stakeholders for practical applications.

2. LITERATURE REVIEW

2.1. Water contamination

The world is facing formidable challenges in meeting rising demands of clean water as the available supplies of fresh water are decreasing due to (i) extended droughts, (ii) population growth, (iii) more stringent health based regulations, and (iv) competing demands from a variety of users for domestic purposes, industry, and irrigation [10]. These factors cause biological pollutants, microorganisms, and solid wastes. Persistent organic pollutants, such as polycyclic aromatic hydrocarbons, polychlorinated biphenyls, pesticides, various industrial additives and pharmaceutical and personal care products are ubiquitous in nature [11]. The presence of organic matters and traces of its accumulation in waste water continues to pose a health risk to humans and aquatic environments; and the present day technologies such as coagulation/flocculation and chlorine technologies are unable to yield satisfying results. Additionally, these processes generate extra volumes of sledges which need further treatment and disposal [10-14].

There has been an ever increasing need for the global community to develop efficient and affordable technologies to improve the quality of water to meet human and environmental needs. In recent years, nonmaterial based technologies have emerged as promising alternatives to current water treatment techniques at lower costs and high efficiencies that can, at the same time, meet the increasingly stringent water quality standards. Thus, three major applications of nanotechnology in the fields of environment are namely (1) restoration (remediation) and purification of contaminated material, (2) pollution detection (sensing and detection) and (3) pollution prevention. With the rapid increment of pollutant species and concentration, the development of technologies that able to treat and prevent it is necessary [15].

2.2. Nanomaterials and their synthetic methods

Nanomaterials are materials that are made in nanometer scale (1-100 nm). Nanotechnology is the science of small and dedicated to the production, design and characterization of ultra-small particles with improved properties that has broad application in pharmaceutical, medical, chemical and engineering sciences [12, 16-18].

There are numerous methods that have been reported for synthesis of nanoparticle (Figure 1) such as co-precipitation, thermal decomposition of organic iron precursor, sol–gel method, Polyol

method, surfactant or polymer-assisted precipitation including reverse micelle, co-polymer templates assisted synthesis, solvothermal synthesis and hydrothermal synthesis [5,17,28-29].

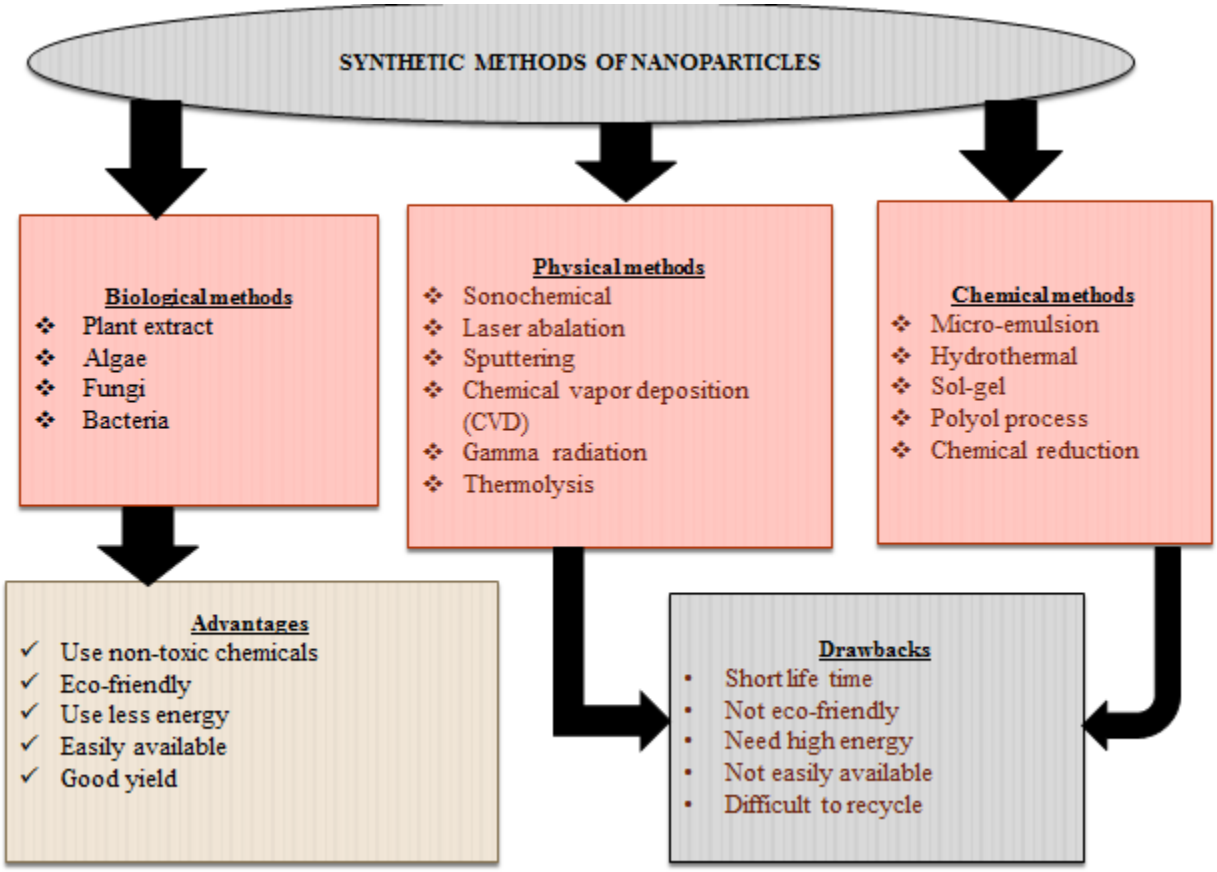

Figure 1. Nanoparticle synthetic methods [17]

Chemical and physical methods have employed the chemicals such as sodium borohydride, diethyl formamide, hydrazine and carbon monoxide as reducing agents and also they are highly reactive and have both biological and environmental negative effects. Therefore, it is highly desirable to prepare Fe_3O_4 NPs via green synthesis approach using non-toxic, environmentally benign materials, which offers numerous benefits of eco-friendliness and compatibility for pharmaceutical, biotechnological and biological applications [29, 30]. Different researches have been conducted before using plant extracts like from *Glycosmis mauritians* leaf extract, *Zanthoxylum armatum* DC leaf extract, *Musa Oranata* flower extract, *Kappaphycus alvarezzii* leaf extract and *Borassus flabellifer* seed extract [31].

This method is beneficial because the catalyst is easily separated by magnet and recyclable without significant loss of activity. The reaction in this synthesis is carried out under mild condition with excellent yields [5, 29].

There are different core factors that affect the formation of plant extract metal nanoparticles. These are time, pH, temperature, reaction environment, concentration of metal ion or metal salt, and metal precursors to extract volume ratio [30].

2.3. Application of iron oxide nanoparticles

A wide range of nanomaterials has the characteristics of catalysis, adsorption, and high reactivity [19]. The change in properties is due to two main effects: (i) surface effects or size reduction effect (ii) quantum confinement-modification in electronic structure [20]. In the recent years, there has been a great focus on nano- sized semiconductors in optoelectronic, catalytic membranes, nanosorbents, bioactive nanoparticles and metal nanoparticles, agriculture, in water and wastewater treatment, restoration, detection and pollution prevention (Figure 2) [16,20-23].

Among various materials, iron oxide nanoparticles (Fe_2O_3 and Fe_3O_4) have received a lot of attention due to their small band gap, high stability and low cost [24-27]. Colloidal iron oxide nanoparticles demonstrate a great potential for applications ranging from metallurgical processing and wastewater treatment, medical and biotechnology, energy storage, and catalysis. The narrow band gap of iron oxide makes it suitable for photoconductive and photothermal applications. In addition to this, the nano iron oxide has been used in drug delivery, biosensors, energy devices, printed electronics, photocatalysis and smart materials [5, 24, and 27].

Magnetic iron oxide nanoparticles (Fe_3O_4 NPs) differ from other iron oxide nanoparticles due to the presence of both Fe^{2+} and Fe^{3+} combinations, where divalent ions are organized at the octahedral sites and trivalent ions are split across the tetrahedral and octahedral sites. The better colloidal stability, biocompatibility, low toxicity, biodegradability, long retention time and persistence magnetic properties of Fe_3O_4 NPs, make them an excellent candidate for biomedical applications for detection of biomolecules like Ascorbic acid (AA), glucose, proteins, urea, and uric acid [7].

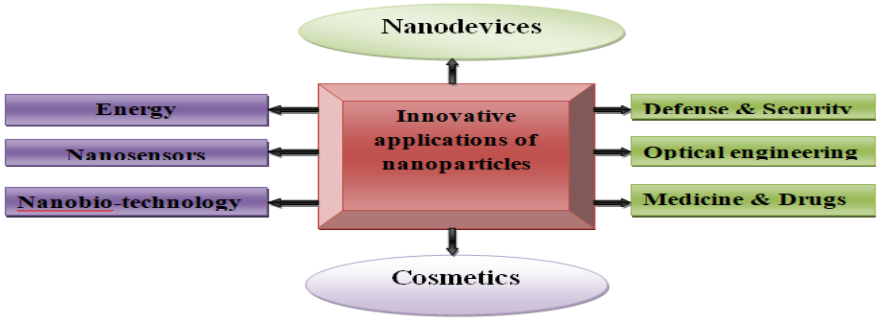

Figure 2. Innovative applications of nanoparticles [16]

2.4. The Nature of *Maesa lanceolata* L.

A *Maesa lanceolata* L. is a shrub or small tree about 5 m with simple, wide oval, usually up to 10 cm long, shiny green above, pale below, thick and leathery, the edge well toothed, tip pointed, a leaf stalk 2–3 cm, often yellow leaf. Bioactive compounds such as phenols, terpenoids, anthraquinones, flavonoids, saponins and alkaloids are present on the leaf, roots and stem bark extracts of the plant (Figure 3) [8-9, 11].

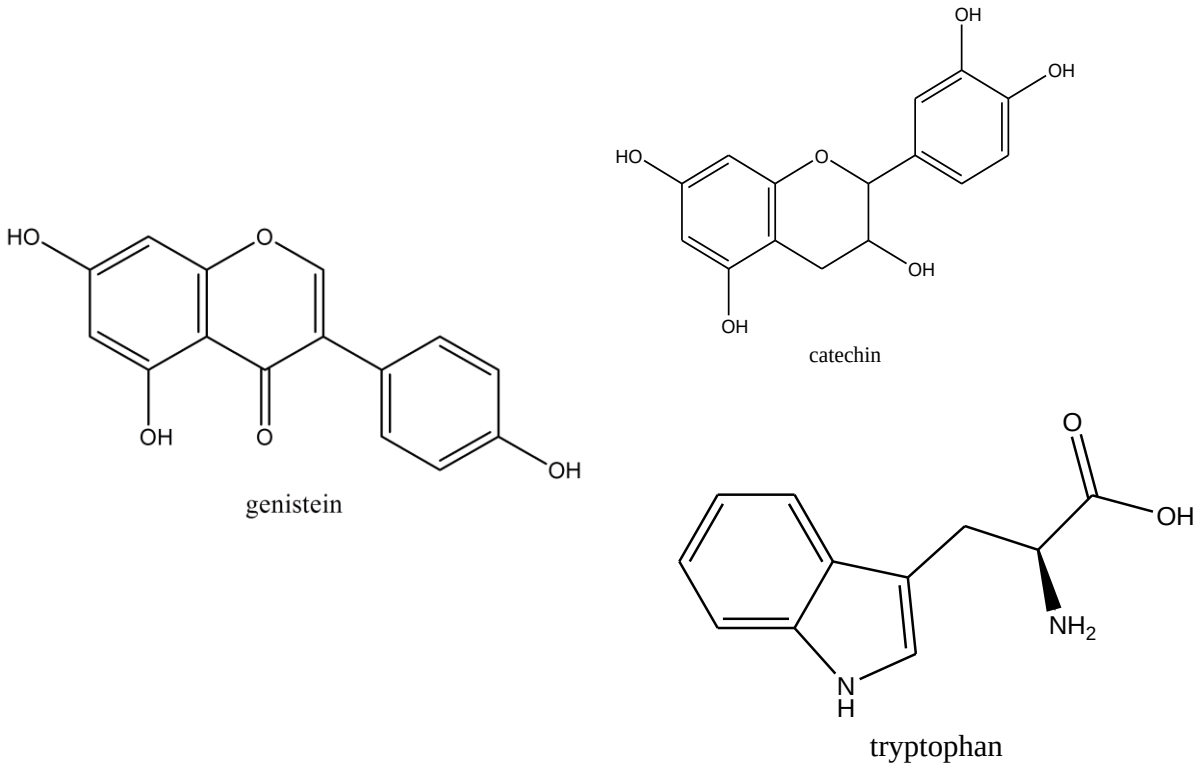

Figure 3. The main types of secondary metabolites present in *Maesa lanceolata* L.

In Ethiopia, it occurs in gallery forest, dry evergreen forest margins, and woodlands and on mountain slopes with *Acacia*, *Carissa*, and *Euclea*.

It has, for example, been recorded in Debre Marks and Yogof State Forests. It grows well in Moist and Wet Weyna Dega and Dega agro climatic zones in nearly all regions, 1,500-3,000 m. In Ethiopia, traditionally its yellow fruit and leaf yield oil which is used to grease new pottery as water proofing agent and traditional medicine [11].

2.5. The role of secondary metabolites in Plant Extract capped green synthesis of NPs

Synthesis of NPs using plant extract has been reported in several plant species. A wide range of molecules, ranging from proteins to various low molecular weight compounds such as terpenoids, alkaloids, amioacids, alcoholic compounds, polyphenols (catechin, flavones, taxifolin, procyanidins), glutathiones, polysaccharides, antioxidants, organic acids, quinines etc. have been reported to play a role in the green synthesis of NPs (Figure 4). The participation of sugars, terpenoids, polyphenols, alkaloids, phenolic acids, and proteins in the reduction of metal ions into NPs and in capping their subsequent stability has also been postulated. Fourier-transform infrared spectroscopy (FT-IR) analyses have been used to obtain clues on the biomolecules possibly involved in the reduction of the metal ions and capping. The secondary metabolites present in the plant extract have ability to donate electrons to the metal ions and convert them to NPs. Of all the secondary metabolites, flavonoids can form a ring structure (chelating properties) with the metal oxide and form a very stable particle. Flavonoids act as poly dentate ligand during NPs synthesis. Therefore, flavonoids have been the compounds most commonly reported to participate in the green synthesis [6].

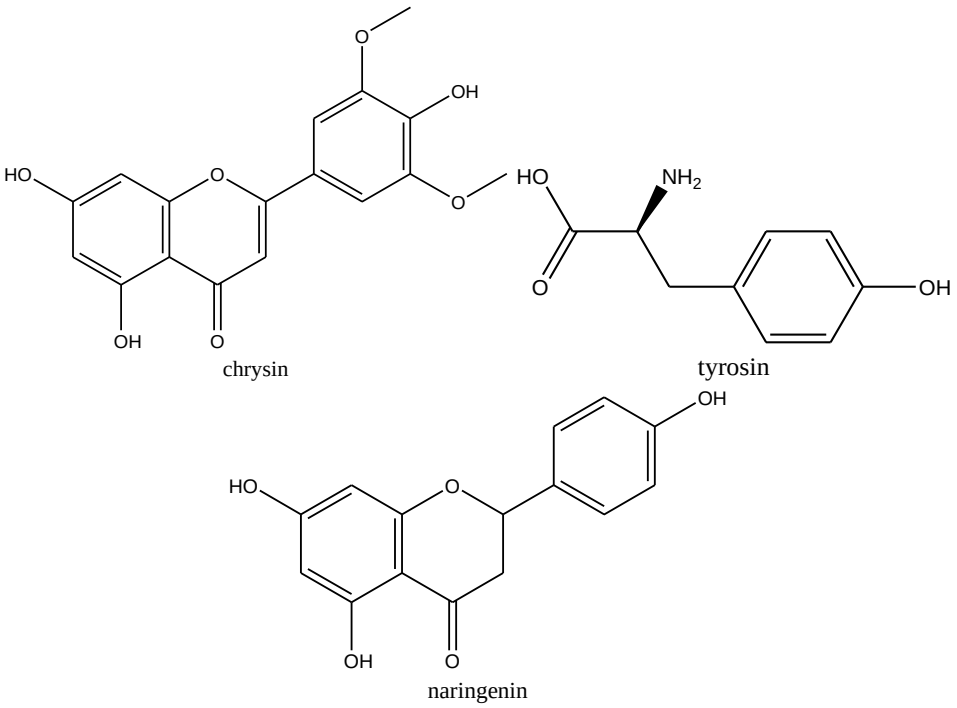

Figure 4. Common flavonoids [6]

2.6. Dyes and photocatalytic dye degradation

A dye is a colored substance that chemically bonds to the substrate to which it is being applied. This distinguishes dyes from pigments that do not chemically bind to the material they color. Dyes are the best choice for totally transparent products. Safranine, Crystal violet (CV), Methylene blue (MB), Congo red (CR) and Eosin are common examples of coloring dyes. Azo dyes are numerically the most important class of dyes, since more than 50% of all dyes listed the color index are azo dyes. Dyes possess color because they: absorb light in the visible spectrum (400-700 nm), have chromospheres, have a conjugated system and exhibit resonance of electrons. Dyes are used in different industries for coloring purposes. [2, 17]

Dyes effluent disposal from different industries are sources of pollution of rivers and waterways. Many dyes and their breakdown products are carcinogenic, mutagenic and toxic to life. They are highly soluble in plastics. Most coloring, dyes are thermally stable. They are not readily degradable and are typically not removed from water by the waste water treatment system and conventional techniques like adsorption, ultra filtration, chemicals, and electrochemical methods. Among all the non-biodegradable stuffs, MB (cationic dye with a chemical formula of $C_{16}H_{18}ClN_3S$) is a commonly used dye stuff that has wider applications including coloring textiles, paper, leather, rubber, soap and detergents, drugs and others (Figure 5).

However, acute exposure to MB will cause health problems such as, increasing heart rate, vomiting, shock, cyanosis, and tissue necrosis in humans [1-2].

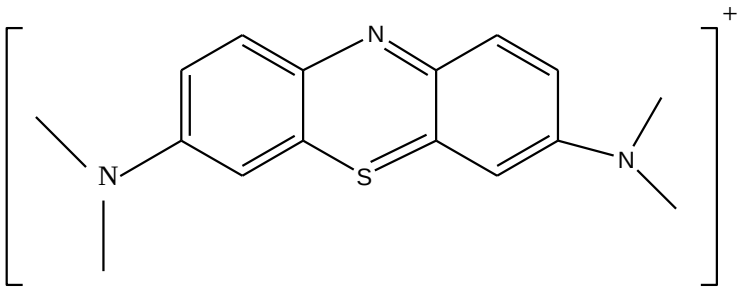

Figure 5. The chemical structure of methylene blue dye

In the past, several physical techniques like photodegradation, coagulation, flocculation, reverse osmosis, adsorption on the activated carbon, ion exchange method ultra-filtration and chemical methods like photosensitized oxidation, adsorption, have been used to reduce the toxic dye effluents from waste water though methods are fairly effective in removing pollutants [31].

However the main drawback of these techniques is formation of secondary waste product which cannot be treated again and dumped as such [31-35].The use of advanced oxidation processing offers a potential solution for industrial wastewater treatment. This approach is based on producing activated species such as hydroxyl radical that will react with and purify a wide range of industrial pollution. One type of advanced oxidation processing methods uses Fe_3O_4 NPs. High photocatalytic function, long durability, and high oxidation rates by holes in the band structure, relatively low price, being non-toxic and anticorrosion against light and chemicals are some advantages of using Fe_3O_4 NPs as a photocatalyst.

Fe_3O_4 NPs are activated *via* light energy which is higher than their band gap energies. Therefore, Fe_3O_4 NPs can be activated by spectrum of direct sunlight. Under such conditions, conduction band electrons and valence band holes are developed. These developed electrons participate in a reduction reaction of oxygen in the air adsorbed on the surface of the Fe_3O_4 NPs and converts them into superoxide anion radical ($O.^{2-}$). Holes present in the valance band degrade existing water molecules to hydroxyl radicals (.OH). The hydroxyl radicals participate in oxidation reactions with pollutant dyes that have organic functional groups and degrade them into less harmful materials to the environment e.g. water and carbon dioxide [36-40].

The photocatalytic degradation involves several steps such as adsorption-desorption, electron-hole pair production, recombination of electron pairs, and chemical reactions as given in the following pathways [40].

Fe_3O_4 NPs + hv → e_{CB}^- + e_{VB}^+ ..... **(1)**

e_{CB}^- + O_2 → $O_2^{\cdot}$ ..... **(2)**

O_2^- + H_2O → $HO_2\cdot$ + OH..... **(3)**

h_{VB}^+ + OH^- → $\cdot OH_{ad}$ ..... **(4)**

h_{VB}^+ + H_2O → $\cdot OH$ + H^+ ..... **(5)**

$\cdot OH$ + MB + O_2 → CO_2 + H_2O ..... **(6)**

e_{CB}^- + h_{VB}^+ → Fe_3O_4 NPs ..... **(7)**

The photocatalytic dye degradation mechanism can be illustrated as given in figure 6 below.

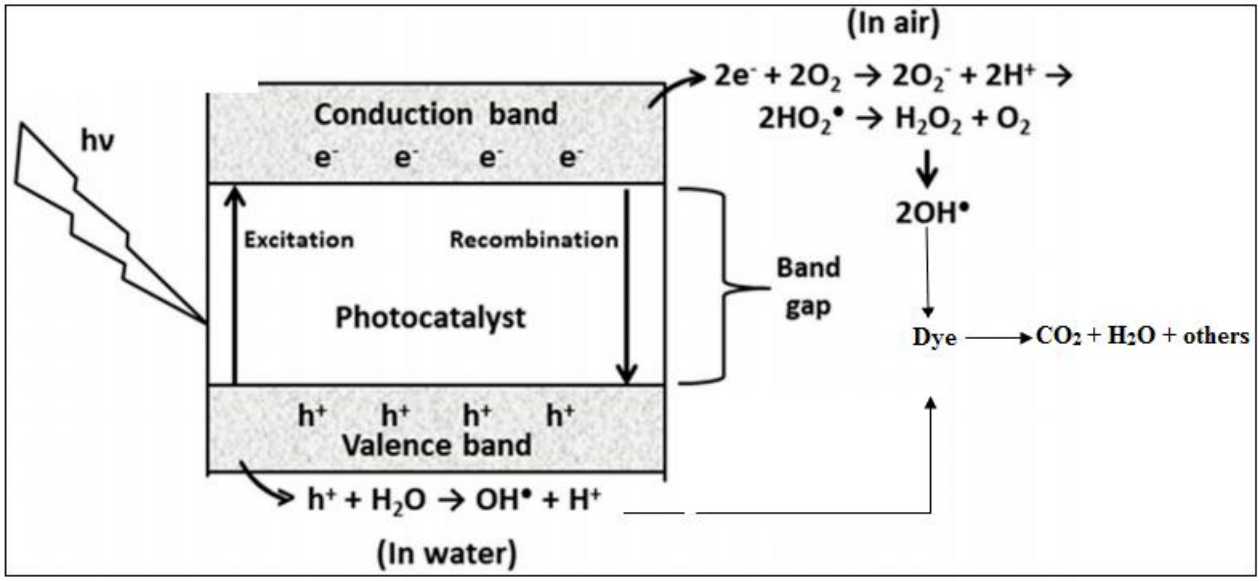

Figure 6. Pictorial representation of photocatalytic dye degradation process

3. MATERIALS AND METHODS OF THE STUDY

3.1. Study area and period

This study was carried out from July 1, 2020 to January 30, 2021 at chemistry research laboratory, Jimma University main campus, which is 346 km south west of Addis Ababa Ethiopia (Appendix 3.1).

3.2. Chemicals and materials

3.2.1. Chemicals

All chemicals used were of analytical grade. Hexahydrated ferric chloride (99.0%, FARDIBAD,INDIA), Tetra hydrated ferrous chloride (98.0%, FARDIBAD,INDIA), H_2SO_4(99%, VWR international , France), Chloroform (Sigma Aldrich, UK), Sodium hydroxide (99.9%, Ranchem industry, Turkey), Hydrochloric acid (38%, Merck, Germany) ,Sodium chloride (99.9%, Loghborough,LE11 5RG, UK), Potassium iodide (99.5%, ALPHA CHEMIKA, INDIA), Iodine (99.9%, ,FARDIBAD,INDIA), Ethanol (98% ± 1%, Ranchem industry, Turkey), Methylene blue (Merck, Darmstadt, Germany).

3.2.2. Materials and equipment

Table top centrifuge (PLC. 02 Taiwan), Hot plate (Stone, Stafford Shire, ST15 OSA, UK), pH meter (Bante 902p, Shanghai. China), Glass beaker, Round bottom flask, Erlenmeyer flask, Volumetric flasks, Evaporating dish, Bar magnet, Measuring cylinders, Oven (model-158005/12, Gallenkamp, UK), Test tubes, Conical flasks, Electronic balance (Adam, AFP-1100, UK),Water bath (Grant GLS 400,England).

3.3. Characterization instruments

Analytical instruments used for this study were UV-Vis Spectroscopy double beam (Analytikjena-ASpectUV-1.2.3.6173, resolution 1 nm between 300 and 600 nm. JENWAY-ST15OSA), UV-Vis Spectroscopy single beam (JENWAY model6705 UK), FT-IR (Perkin Elmer spectrum two, model L1600300 spectrum two LITA, Liantrisant, UK scan rate from 4000 to 400 cm^{-1}) and XRD (Schimadzu-7000 , U.S.A. scanning rate 0.030, 1º/sec resolution, counter intensity 5000).

3.4. Methods

3.4.1. Collection of the *Maesa lanceolata* L. leaf

Maesa lanceolata L. leaf were collected from the local garden near Bonga University, which is located in the SNNP region in Ethiopia, Kaffa Zone at a distance of 449 km from the capital Addis Ababa and 110 km to south from Jimma town (Appendix 1,2), and it was transported to Jimma University Inorganic Chemistry Research Laboratory.

3.4.2. Extraction of aqueous leaf extract

The plant leaf extraction was done according to previously reported literature [1] as follows. The leaf were repeatedly washed with distilled water and dried under shade in an open-air, protected from direct exposure to sunlight for about two weeks. The dried plant sample was ground using coffee grinder and stored in airtight container and used as reducing and stabilizing agent for synthesis of Fe_3O_4 NPs. About 20 g of the ground powder sample was soaked by maceration technique using 200 mL distilled water in a separated 500 mL Erlenmeyer flask for 24 h using a water bath at room temperature. Then, the resulting extract was filtered out through Whatman No. 1 filter paper, which was adjusted to the large funnel. The aliquot was kept under 4 $^{\circ}$C temperature for not more than two weeks and used for further experiments.

3.4.2.1. Phytochemical screening test

The phytochemical screening test was conducted based on previous work [39].

1. **Test for sterols/terpenes**

Salkowski test: About 2-3 mL of the extract was dissolved in 1 mL chloroform and to it 1 mL of concentrated sulfuric acid was added in the test tube to form two phases. Formation of reddish brown coloration was taken as an indication for the presence of sterols.

2. **Test for flavonoids**

Sodium hydroxide test: Two mL of the extract was dissolved in 10% aqueous sodium hydroxide solution and filtered to give yellow color, a change in color from yellow to colorless on the addition of 2-3 drops of dilute hydrochloric acid was used as an indication for the presence of flavonoids.

3. Test for alkaloids

Wagner's reagent was prepared by dissolving 1 g of I and 5 g of KI in 100 mL volumetric flask using distilled water.

To 3 mL of filtrate, 1 mL of Wagner's reagent was added. The appearance of reddish brown precipitate indicates the presence of alkaloids.

4. Test for tannins

About 5 mL of the extract was boiled with water and filtered. Two drops of ferric chloride solution were added into the filtrate, formation of a blue-black, or green precipitate was taken as evidence for the presence of tannins.

5. Test for saponins

Froth test: About 5 mL of the extract was shaken in about 5 mL of water in a test tube. Frothing which persisted for 15 min indicates the presence of saponnins.

6. Test for Phenolic

Ferric chloride test: The development of dark green color in addition of a few drops of neutral ferric chloride to the extract was the indication of the presence of the phenolic compounds.

7. Test for Glycosides

Brown ring test: Formation of brown ring at the interface by the addition of 2 mL of glacial acetic acid followed by a few drops of ferric chloride solution and 1 mL of concentrated sulfuric acid to the extract reveals the presence of glycosides.

3.4.3. Synthesis of Fe_3O_4 NPs by plant extract

Fe_3O_4 NPs were synthesized *via* green synthesis method in the presence of aqueous leaf extract of *Maesa lanceolata* L. as a reducing and capping agent as described in other the report with careful optimization of different Physico-Chemical parameters [37-38]. In brief, 1.11 g of Ferric chloride hexahydrate ($FeCl_3.6H_2O$) and 0.53 g of ferrous chloride tetra hydrate ($FeCl_2.4H_2O$) (2:1 molar ratio) were dissolved in 100 mL of distilled water in a 250 mL beaker. Then, the solution was heated at 80 $^{\circ}$C using magnetic stirrer in a closed system for about 30 min and cooled to room temperature.

After 10 min, 5 mL of the aqueous solution of *Maesa lanceolata* L. leaf extract was added to the above solution drop wise. Brown colored suspensions formed gradually. After 5 min, about 5-7 mL of 0.2 M NaOH was added drop wise for allowing the magnetite formation uniformity. From the first addition of NaOH the reddish brown color of the suspensions of magnetite changed to black. The mixture was allowed to cool down to room temperature and the Fe_3O_4 NPs were obtained by decantation. The Fe_3O_4 NPs were purified by dispersing in distilled water and centrifuged at 4500 rpm three times.

Optimization of various physicochemical parameters for Fe_3O_4 NPs synthesis

Several physico-chemical parameters were optimized including pH, concentration of metal ions, the volume of the plant extract and reaction time to synthesize Fe_3O_4 NPs as reported in other literature [41].

1. **Effect of pH**

PH of the synthesized Fe_3O_4 NPs was maintained at 3, 8, 10 and 12 by using either 0.1 M NaOH or 0.1M HCl. The absorption of each Fe_3O_4 NPs solution was measured by the UV-Vis spectrophotometric approach. The pH of the solution with sharp peak at 370 nm was taken as optimum pH.

2. **Effect of reaction time**

The reaction time for the formation of Fe_3O_4 NPs was optimized by measuring its UV-Vis spectroscopic measurement at room temperature at the reaction time intervals at 2, 5, 7 and 10 min using the same procedure as stated in No.1 above.

3. **Effect of volume of plant extract**

The volume of the plant extract was maintained by taking 3 mL, 4 mL, 5 mL and 6 mL using measuring cylinder to synthesize Fe_3O_4 NPs. Then the volume of the plant extract was optimized by measuring the UV-Vis absorbance of the synthesized Fe_3O_4 NPs by varying the volume of the plant extract.

4. **Effect of molar ratios of metal ions**

The concentration of metal ions was optimized by taking different molar ratios of $FeCl_3.6H_2O$ to $FeCl_2.4H_2O$ (2:1, 1:2 and 1:1 respectively) and synthesizing the NPs by adding 5 mL of the plant extract. The molar ratio of the metal ions was optimized by measuring the UV-Vis spectroscopic measurement of each product.

5. Effect of reaction temperature

The reaction temperature was maintained by keeping the temperature of each system at 25 ºC, 40 ºC and 60 ºC. The UV-Vis spectroscopy of each of the Fe_3O_4 NPs at the indicated point of temperature was measured and the reaction temperature was optimized.

3.4.4. Characterization of magnetic iron oxide (Fe_3O_4) nanoparticles

The preliminary characterization of nanoparticles was studied after recovering the embedded nanoparticles from the plant matrix using UV-Vis spectrophotometer to study the band gap energy and electron transition of the nanoparticles. The band gap energy (E_g) of Fe_3O_4 NPs was determined from the UV-Vis spectra by Tauc plot of $(h\nu\alpha)^2$ versus ($h\nu$) and extrapolation of the linear portions of the curves to the energy axis:

$$(\alpha h\nu)^2 = \beta\,(h\nu - E_g) \quad \text{---------- (1)}$$

where α is the absorption coefficient, $h\nu$ is the photon energy, E_g is the direct band gap energy, and B is a constant. The absorption coefficient (α) was determined from the relation $A = I/I_0$ or it can be calculated using the well-known relation deduced from Beer–Lambert's relation, $\alpha = 2.303A/d$, where A is the absorbance determined from the UV–visible spectrum and d is the path length of the quartz cuvette.

X-Ray Diffraction (XRD) analysis was used to identify the crystalline formation and estimated average crystalline size of the resultant Fe_3O_4 NPs. Based on the XRD data, the average crystalline sizes of the Fe_3O_4 NPs was calculated from the full width at half maximum (FWHM) of the characteristic diffraction angle by the Debye–Scherer's equation [44].

$$D = k\lambda/\beta\cos\theta \quad \text{---------- (2)}$$

Where D is the crystalline size, k=0.94 is a constant shape factor, λ is the X-ray wavelength for Cu Kα (1.54178 Å), β is the full width at half maximum obtained by using origin pro 6 software in radians and θ the Bragg's angle in radians.

Fourier Transform Infrared Spectroscopy (FT-IR) analysis was done over the range of wave number 4000 cm^{-1} -400 cm^{-1} to examine the property of functional groups present on the surface of Fe_3O_4 NPs [1].

3.4.5. Determination of point of zero charge (PZC) of Fe_3O_4 NPs

For the determination of PZC of Fe_3O_4 NPs pH drift method was adopted with little modification from previous report [38]. Briefly, 1 L of 0.1 M NaCl solution was prepared and boiled for about 30 min to separate dissolved CO_2 and then cooled at room temperature. Then, 50 mL of each of the solution was kept in each of 10 different capped 100 mL vials. The initial pH (pH_i) of each of the solution was then adjusted to 3, 5, 7, 9 and 11 (in doublet) respectively by carefully adding the required amount of either 0.1 M HCl or 0.1 M NaOH. Then 30 mg of powdered samples of Fe_3O_4 NPs was added in to each of the solution in a vial, and then capped and placed in the shaker for 48 h for stabilizing the pH. After 48 h of shaking the solutions in each vial was filtered and the final pH (pH_f) of each of the solutions containing the indicated amount of Fe_3O_4 NPs was measured the average of the doublet was taken. Finally, a graph is plotted against initial pH versus change in pH (Δ pH) to calculate PZC. The point of the curve at which it crosses the X-axis was taken as the point of zero charge of Fe_3O_4 NPs according to previously reported literatures [38].

3.4.6. Evaluation of catalytic dye degradation of Fe_3O_4 NPs

The experiments were carried out in three different conditions (in solar irradiation without any catalyst (photolysis), with catalyst in dark (dark reaction) and in the presence of Fe_3O_4 NPs (nanocatalyst) in solar irradiation (photocatalysis).

At the beginning, 1L of 10 mg/L MB solution was prepared and kept carefully in dark room. To evaluate the degradation of MB solution in the absence of nanocatalyst in solar irradiation (photolysis), 50 mL of the solution was taken and its absorbance was measured at maximum absorption wave length of MB (at 665 nm) using UV-Vis spectrophotometric measurement by taking about 3 mL of the liquate and recorded. Then, the solution was subjected to solar irradiation for about 90 min while continuous stirring and its concentration variation was measured at every 10 min of time interval and the result was analyzed.

The degradation efficiency of Fe_3O_4 NPs was calculated using the following formula:

$$D = \frac{A - At}{A} \times 100 \quad \text{……………………………… (3)}$$

where D is degradation efficiency of Fe_3O_4 NPs, A is initial absorbance and A_t is absorbance at any time after solar radiation.

To evaluate the degradation of MB in the presence of nanocatalyst in the dark (in the absence of solar irradiation), 50 mL of 10 mg/L of MB dye 30 mg of nanocatalyst was added and stirred using magnetic stirrer in the dark for 1 h until complete adsorption/desorption equilibrium [39]. After 1 h of continuous stirring in the dark aliquots of approximately 3 mL was taken and centrifuged at 4000 rpm for 5 min. Then, the supernatant was analyzed using UV–Vis spectrophotometer to determine its initial concentration (C_0). At this moment, the time was taken as t_0 (t_0=0). And the dark reaction absorbance was recorded after every 10 min and its concentration (C at a given time t) was recorded for 90 min while continuous stirring in the dark (dark reaction). To evaluate the photocatalytic degradation of MB by nanocatalyst in the presence of solar irradiation, to 50 mL of 10 mg/L MB, 30 mg Fe_3O_4 NPs was added in test sample. The suspension was stirred thoroughly using magnetic stirrer in the dark for 1 h to maintain the adsorption/desorption equilibrium [42]. After 1 h of continuous stirring in the dark aliquots of approximately 3 mL were collected and centrifuged at 4000 rpm for 5 min. Then, the supernatant was analyzed using UV–Vis spectrophotometer and the initial concentration of MB was recorded. Then, the solution was subjected to solar irradiation in an open atmosphere. Then, the concentration of MB solution was measured after every 10 min of time intervals while continuous stirring in solar irradiation by taking aliquots of 3 mL of the solution using UV-Vis spectrophotometer in the same procedure while the de-colorization of the dye was observed.

This experiment was repeated thrice and the average result was recorded. Then, the graph of C/C_0 versus time (min) was plotted.

3.4.6.1. Parameters affecting the efficiency of the MB degradation

Important parameters affecting the photocatalytic degradation of MB by Fe_3O_4 NPs were described below as illustrated in other study [37].

1. **The pH of the solution**

To study the effect of pH variation of the MB solution, a series of solutions containing the concentration of MB (5 mg/L) and 30 mg of Fe_3O_4 NPs were adjusted at pH 4, 8, 10 and 12 respectively using 0.1 M HCl and 0.1 M NaOH in aqueous medium. Then, the pH effect was studied by measuring the concentration variation of each solution after stirring in the dark for 1 h and subjecting to solar irradiation.

Then, concentration of each solution was measured after every 10 min for about 90 min and recorded by taking 3 mL of the aliquot and centrifuging for 5 min. This experiment was done by keeping other parameters constant. At the end the experiment, the graph of C/C_0 vs Time (min) was plotted to describe the effect of pH on degradation of the dye.

2. Effect of the initial dye concentration

To evaluate the initial concentration dependence on degradation of MB, in each of the different concentration of MB (2.5 mg/L, 5 mg/L, 7.5 mg/L and 10 mg/L), 30 mg of the photocatalyst was added and stirred in the dark for 1 h. Then, after 1 h of dark equilibration about 3 mL of the aliquots of each solution was taken and centrifuged at 4000 rpm and then its absorbance was measured to calculate the initial concentration of each solution from Beer lambert law as described in No. 1 above..

3. The effect of mass (dose) of the photocatalyst (Fe_3O_4 NPs)

The dependence of the photocatalytic degradation of MB on the mass of the nanocatalyst was studied by taking each of the 10 mg, 20 mg, 30 mg, 40 mg and 50 mg of the nanocatalyst in five different beakers containing 50 mL of 5 mg/L MB dye and keeping in dark for 1 h while continuous stirring. Then, the concentration of each solution was measured after subjecting to solar irradiation by keeping other parameters constant using the same procedure as given in No.1 above.

4. Effect of temperature

To study the impact of temperature variation on photocatalytic degradation of MB, the reaction was conducted by fixing 50 mL of 5 mg/L of MB dye containing 30 mg of the photocatalyst at four different temperatures (25 $^{\circ}$C, 40 $^{\circ}$C, 60 $^{\circ}$C) and keeping in the dark for 1 h while continuous stirring. Then, the degradation efficiency was measure by keeping other factors constant in the same procedure as given in No. 1 above.

3.4.6.2. Reusability of the catalyst

After photocatalytic degradation experiments, the nanocatalyst used in the degradation experiment was isolated from the solution using a magnet and washed with distilled water three times with successive centrifugation at 4000 rpm.

After washing and successive centrifugation, the recovered photocatalyst (Fe_3O_4 NPs) was dried in an oven for about 7 h and its recoverability and successive degradation efficiency was checked for three runs [38].

4. RESULTS AND DISCUSSION

4.1. Extraction and observation inferences

Maesa lanceolata L .leaf was extracted by collecting, drying and grounding into powder. Then, 20 g of the dried leaf powder was soaked in 200 mL of distilled water and put in a water bath for about 24 h. The extract was filtered by Whatman No. 1 filter paper and yellowish brown colored extract was obtained (Appendix 3) [1].

4.1.1. Phytochemical screening

The crude extract of *Maesa lanceolata* L. leaf obtained from cold extraction using distilled water was used to investigate preliminary phytochemical studies [39]. The extract was subjected to various qualitative tests to identify the presence of different secondary metabolites or phytoconstituents such as alkaloids, flavonoids, terpenoids, tannins, Phenols, Saponins and glycosides [1, 45] (Appendix 4).

The results of the phytochemical screening test for aqueous extracts of *M. lanceolata L.* leaf were summarized (Table 1).

Table 1. The phytochemical screening test for aqueous extract of Maesa lanceolata L. leaf

Phytochemicals	Aqueous extract
Terpenes	+
Flavonoids	+
Alkaloids	+
Tannins	+
Saponnins	+
Phenols	+
Glycosides	+

+ indicates detected, — indicates not detected

The presence of these phytochemical compounds that may contain the functional groups like OH, C=O, N=H, C=C etc. used as reducing and capping agents in the synthesis of Fe_3O_4 NPs.

4.2. Synthesis and optimization of Fe_3O_4 NPs

In this study, *Maesa lanceolata* L. leaf extract was used as reducing and stabilizing agent for the green synthesis of Fe_3O_4 NPs. The synthesized Fe_3O_4 NPs were subjected to UV-Vis spectroscopic measurement. The absorption peak was observed at 370 nm wavelength. The formation of Fe_3O_4 NPs is influenced by several factors like pH, the volume of the plant extract, the concentration of metal ions, time of the reaction and reaction temperature as indicated in table 2 (Appendix 5-10).

Table 2. Optimization parameters on synthesis of Fe_3O_4 NPs

Parameters	Amounts used	Optimization
pH	3.0, 8.0, 10.0 and 12.0	10.0-12.0
Volume of plant extract	3 mL, 4 mL, 5 mL and 6 mL	5 mL
Concentration ratio of the metal salts ($FeCl_3.6H_2O$ and $FeCl_2.4H_2O$)	2:1, 1:2 and 1:1	2:1
Temperature	25 $^{\circ}$C, 40 $^{\circ}$C and 60 $^{\circ}$C	20 $^{\circ}$C-40 $^{\circ}$C
Time of reaction	2 min,5 min, 7 min and 10 min	10 min

4.3. Characterization

4.3.1. UV-Vis spectroscopy analysis

The formation of iron nanoparticles was characterized by measuring their absorbance with UV-Vis spectrophotometer over the range from 300 to 800 nm. The synthesized Fe_3O_4 NPs have the absorption peak at 370 nm (Figure 7).

According to Tauc's relation, the plotting of $(\alpha hv)^2$ versus the photon energy (hv) gives a straight line in a certain region. The extrapolation of this straight line will intercept the (hv) -axis to give the estimated value of the optical band gap energy (Eg) as indicated in the figure. Therefore, the intersection value which is 2.9 eV is the direct band gap energy, according to Tauc's Equation [43].

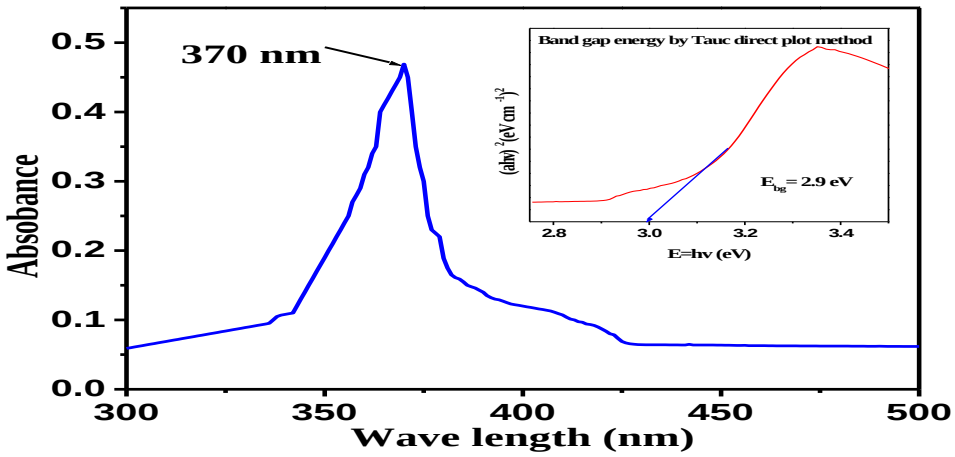

Figure 7. The UV-Vis spectroscopic absorption bands and band gap energy of Fe_3O_4 NPs with Tauc plot inset

4.3.3. Fourier transform infrared (FT-IR) spectroscopy

FT-IR measurements of *Maesa lanceolata* L. leaf extract and the synthesized Fe_3O_4 NPs were carried out to understand the involvement of biomolecules in nanoparticle synthesis as reducing and stabilizing agents. It was performed to determine the functional groups of leaf extract of *Maesa lanceolata* L. that acted as a stabilizing and capping agent in the synthesis of Fe_3O_4 NPs. FT-IR spectra of the plant leaf crude extract and the synthesized nanoparticles are shown in figures 8 and 9.

The spectrum of the extract shows broad peaks at 3439 cm^{-1} may be attributed to OH stretching vibration of the phenolic compounds and overlapped N-H groups present in it, peaks at 2923 cm^{-1}, 2850 cm^{-1} arises due to C–H stretches of alkanes. The band at 1744 cm^{-1} corresponds to C=O stretching vibration. Peaks at1635 cm^{-1} indicate aromatic ring, 1545 cm^{-1}occur due to N–H bend of primary amines and N–O asymmetric stretching vibration in Nitro compounds respectively.

Peaks at 1391 $cm^{-1}$and 1237 $cm^{-1}$are contributed by C–C stretch of aromatic group and C-N stretch of amines respectively. The peak at 1064 cm^{-1}appears due to the stretching vibration of C–O and C–O–SO_3 groups [44].

The synthesized Fe_3O_4 NPs showed peaks at 3330 cm^{-1}, 2915 cm^{-1}, 1617 cm^{-1}, 1454 cm^{-1}, 1246 cm^{-1}, 1069 cm^{-1}, 556 $cm^{-1}$and 423 cm^{-1}.

The shift in the FT-IR peaks of leaf extract of *Maesa lanceolata* L. from 3439 cm^{-1} (attributed to O-H stretch) to 3330 cm^{-1} in the FT-IR spectra of oven dried material indicated involvement of polyphenols from the leaf extract of *Maesa lanceolata* L. in stabilizing of Fe_3O_4 NPs. The peak at 2915 cm^{-1} can be attributed to C –H stretching of aliphatic carbon. Also, involvement of the C = O group can be seen in the peak shift from 1635 cm^{-1} in the leaf extract of *Maesa lanceolata* L. to 1617 cm^{-1} in the oven dried material.

These peaks along with peaks at 1069 cm^{-1} (C-O stretch) indicate that minute quantity of residual carbon of *Maesa lanceolata* L. leaf extract. The bands between 650 cm^{-1} –1000 cm^{-1} in the spectrum of nanoparticles are attributed to C–H bend of alkenes. Two significant new peaks were found at 556 and 423 cm^{-1} in the spectra of synthesized Fe_3O_4 NPs, which is associated with the stretching vibration mode of Fe–O [1].

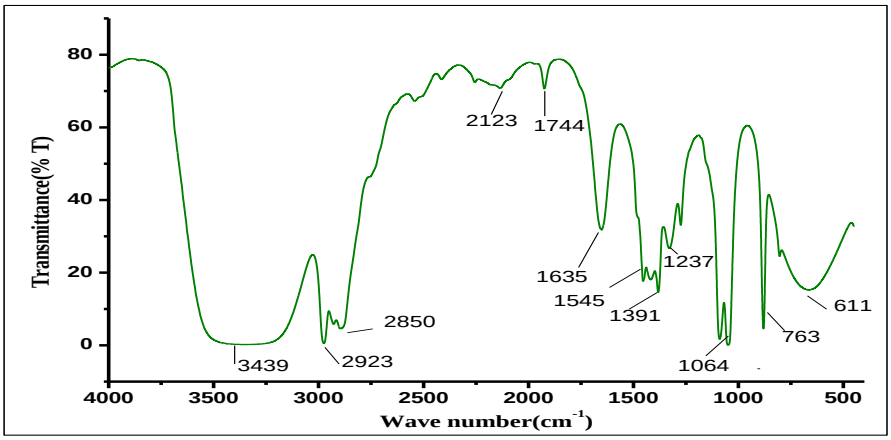

Figure 8. Fourier transform infrared spectra for *Maesa lanceolata* L. leaf extract

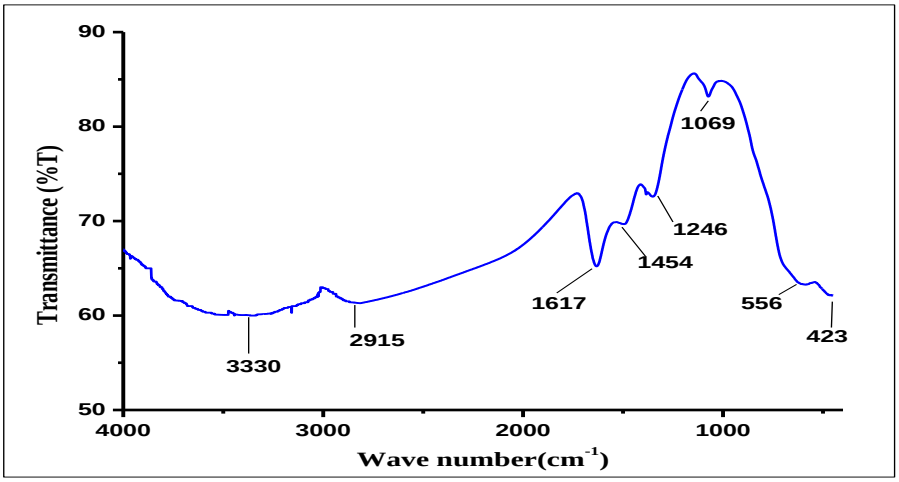

Figure 9. Fourier transform infrared spectra for the green synthesized Fe_3O_4 NPs

4.3.4. X-ray diffraction (XRD) analysis

The phase purity and crystalline nature of Fe_3O_4 NPs were confirmed using XRD analysis. The x-ray diffraction pattern of the Fe_3O_4 NPs shows majorly the presence of magnetite phase and traces of hematite phase as shown in the figure 10. The XRD data clearly confirm the crystalline phase of Fe_3O_4 NPs.

From the X-ray diffraction patterns, six series of characteristic peaks at 2θ = 24.52°, 35.48°, 40.32°,45.72°, 65.2° and 69.6° which correspond to (220), (311), (400), (442), (511) and (440) crystallographic planes of inverse spinel magnetite phase Fe_3O_4 NPs were observed (miller index for each diffraction angles was obtained by using jade 6.5 software).

The analyzed diffraction peaks were matched well with the standard magnetite XRD patterns declared the crystallographic system of cubic structure [41]. Characteristics peak for Fe_3O_4 NPs have been observed at 2θ=35.48°. This broadened diffraction peak suggested the formation of crystalline nanoparticles. The intense reflection of (311) plane in contrast to the other planes may specify the growth direction of the Fe_3O_4 NPs. These findings are analogous with the crystalline nature of Fe_3O_4 NPs [47, 54].The estimated average crystalline size of Fe_3O_4 NPs becomes 14.6 nm.

The observed diffraction peaks indicate, the formation of high crystalline Fe_3O_4 NPs. Similar results for magnetic nanoparticles have been obtained from previous literatures [46, 53].

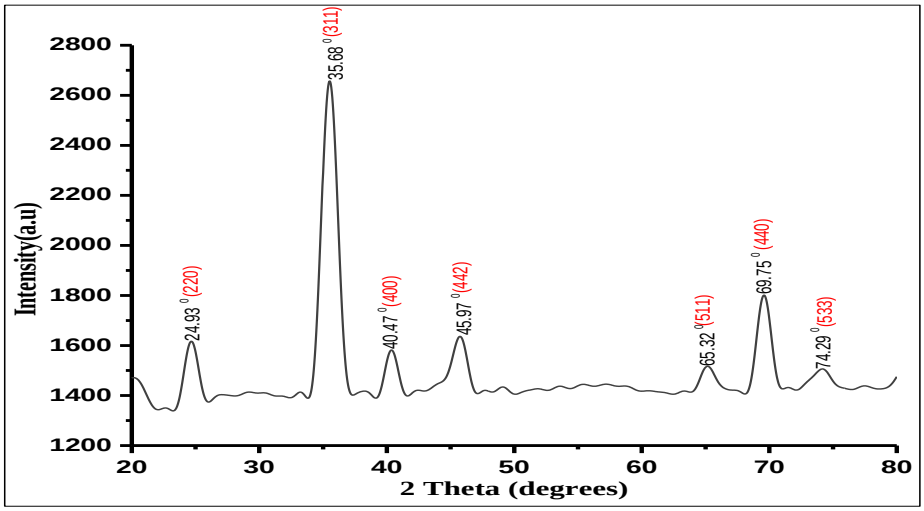

Figure 10.XRD patterns of Fe_3O_4 NPs synthesized by *Maesa lanceolata* L. aqueous leaf extract

4.4.Determination of point of zero charge (PZC) of Fe_3O_4 NPs

The graph for the determination of PZC of Fe_3O_4 NPs is shown in figure 11. The pH curve of the nanoparticles crosses the straight line at X-axis at 6.8 and thus the PZC of the Fe_3O_4 NPs is 6.8. The point of zero charge is the pH at which the surface of Fe_3O_4 NPs is globally neutral, i.e., contains as much positively charged as negatively charged surface functions. Below this value, the surface is positively charged; beyond this value, it is negatively charged. So normally, it is always easier to adsorb a cation on a negatively charged surface, and an anion on a positively charged surface. This value is consistent with the published literature. [38].

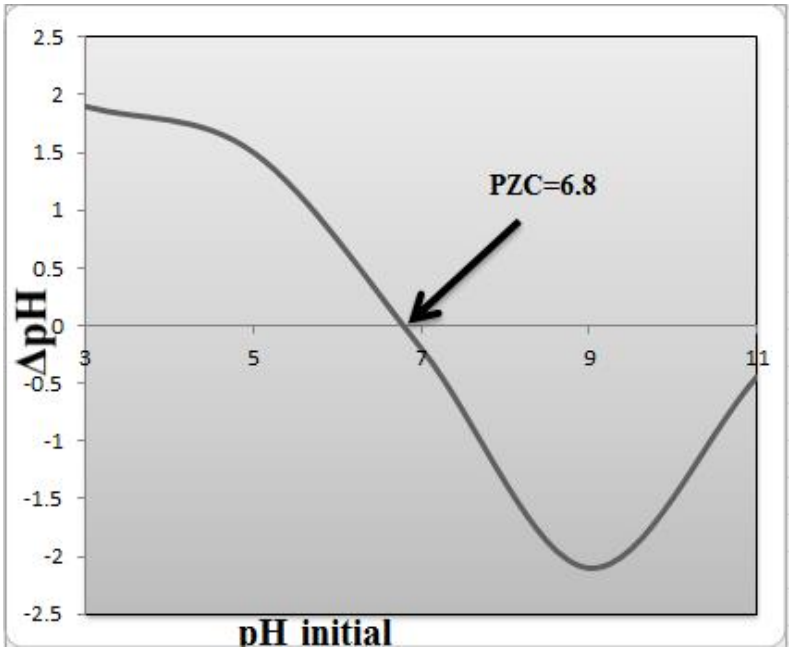

Figure 11. The plot for the determination of PZC of synthesized Fe_3O_4 NPs by *Maesa lanceolata* L. leaf extract (by taking 30 mg of Fe_3O_4 NPs in each of 50 mL of 0.1 M NaCl solution in five capped vials whose pH adjusted to 3, 5,7, 9, and 11)

4.5. Photocatalytic dye degradation of MB

4.4.1. Photocatalytic degradation studies under different conditions

Photocatalytic activities of the synthesized Fe_3O_4 NPs were evaluated by de-colorization of MB in aqueous solution. The experiments were carried out under the visible light irradiation in the presence of Fe_3O_4 NPs as photocatalyst. In the current study, 30 mg of Fe_3O_4 NPs was added at 10 mg/L of aqueous MB solution in 250 mL Pyrex glass beaker. The suspension was magnetically stirred in the dark for 1 h to obtain absorption/desorption equilibrium before irradiating the solution to the light. Then, the solution exposed to solar radiation for about 90 min and the de-colorization of the dye observed (Appendix 11).

The degradation of MB was analyzed using UV-Vis spectrometer. The maximum absorption peak of MB was obtained at 665 nm.

It can be observed from figure 12 a and b (Appendix 12); that the presence of Fe_3O_4 NPs accelerated the degradation of MB with respect to time. From these figures, it could be seen that the intensity of the adsorption peaks diminished gradually as the exposure time increased in the case of using Fe_3O_4 NPs as a photocatalyst which eventually vanished after 80 min.

But in MB degradation without Fe_3O_4 NPs (photolysis), the decrease in intensity of the peaks is very slowly. This is due to the formation of hydroxyl and superoxide radicals on soar irradiated surface of the nanocatalyst which enhances the degradation of MB [45].

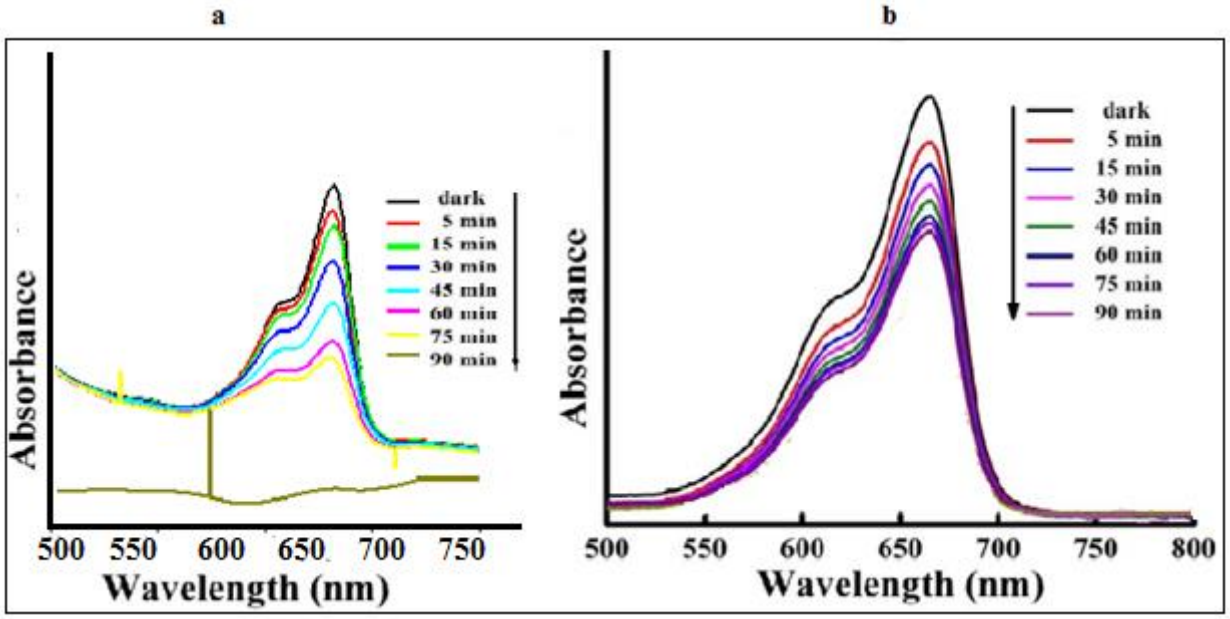

Figure 12. The UV-Vis absorption spectrum of 5 mg/L MB in solar irradiation in the presence of 30 mg of Fe_3O_4 NPs (a) and in the absence of Fe_3O_4 NPs(photolysis)(b) as a factor of time

The degradation of MB dye was also evaluated in the presence of a nanocatalyst without light irradiation (dark reaction) (Figure 13). Degradation of MB in the presence of nanocatalyst increases as a function of time for the first 60 min in the solar irradiation and remains constant through, due to the occupation of the active site of the catalyst and saturation of the solution. This result comes into agreement with previous studies [40, 46].

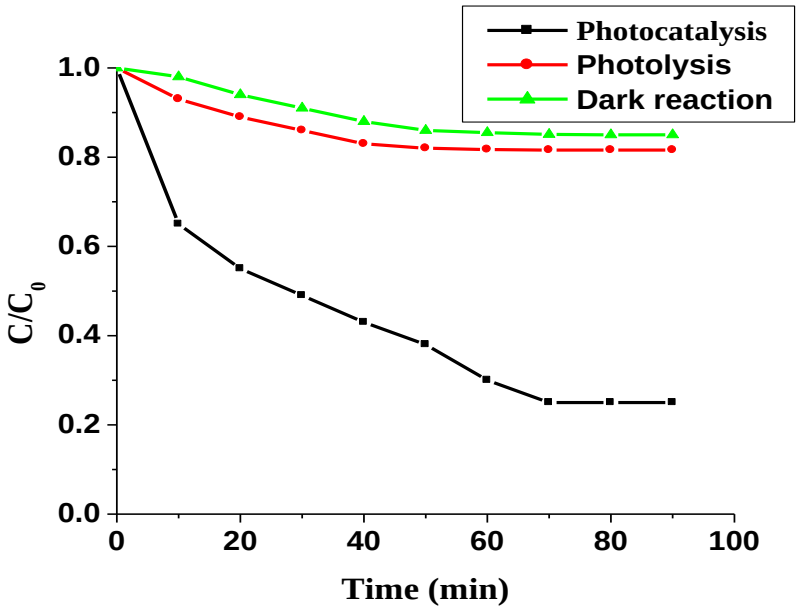

Figure 13. The degradation of MB in the dark and in solar irradiation with photocatalyst and in solar irradiation without photocatalyst (C_0=the initial concentration of MB just immediately after dark equilibrium, C= the concentration of MB at any given time t

4.4.2. Parameters affecting the photocatalytic degradation of MB

To understand the photocatalytic degradation of MB dye using Fe_3O_4 NPs as a catalyst, the influence of several factors on the degradation process, including the initial concentration of the dye, photocatalysis time, photocatalyst mass, solution pH and temperature were studied.

Effect of initial concentration of the dye

Increasing initial dye concentration (the concentration of the dye after 1 h of dark equilibration) at fixed mass of nanocatalyst (30 mg) reduces the photocatalyst degradation efficiency.

As indicated in figure 14 the degradation of MB solution decreases as its initial concentration increases which might be due to the limited number of active sites of Fe_3O_4 NPs and the intermediate formed during the degradation of MB might compete with the MB molecules for the active site [46].

Other possible reason for these results is the effect of UV screening of dye itself. In high dye concentrations a major amount of solar irradiation tends to be absorbed by dye molecules.

This reduces the efficiency of the catalytic reaction due to the decline in .OH and .OH_2 concentrations [50-51].

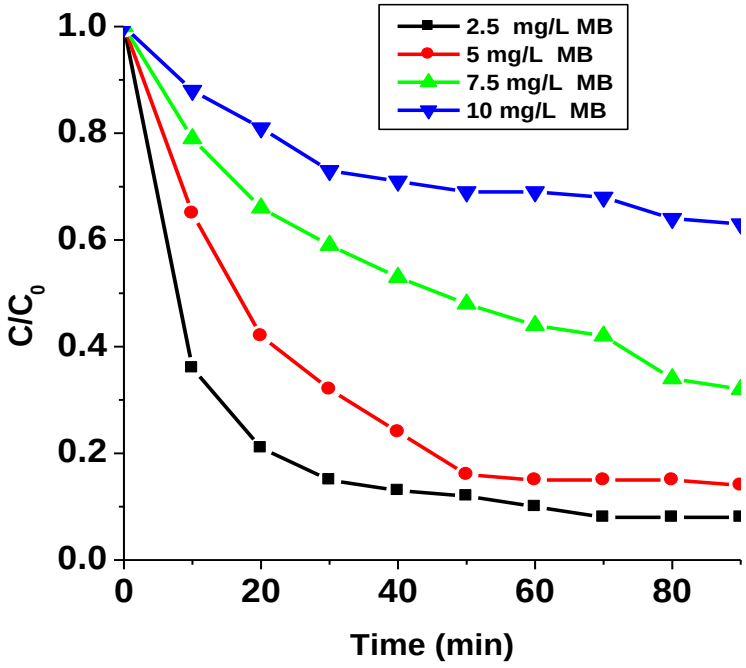

Figure 14. Effect of initial concentration of MB on photocatalytic degradation efficiency of Fe_3O_4 NPs (C_0=the initial concentration of MB just immediately after dark equilibrium, C= the concentration of MB at any given time during photocatalysis

Effect of pH

Since pH of dye solution is a main parameter on the degradation progress, comparative experiments were performed at different pH values (4, 8, 10, and 12). The surface of photocatalyst will be charged negative and results in the increased adsorption of MB (cationic dye) at pH value greater than 6.8 (point of zero charge of Fe_3O_4 NPs). But the degradation of the MB dye is repressed when the pH of the solution is too high (pH $\geq$ 12) (Figure 15) because hydroxyl ions compete with MB for the adsorption on the surface of the catalysts [51]. On the contrary, at low pH (pH<6.8) the adsorption of cationic MB dye on the photocatalyst surface is reduced, because the surface of photocatalyst is positively charged which results in decrease in the adsorption of cationic dye.

So that the degradation efficiency of 30 mg nanocatalyst was 36% at pH 4, 86% at pH 8, 94.1% at pH 10 and 85% at pH 12 for 5 mg/L of MB solution. Thus, the degradation efficiency is declining in lower pH [40, 50].

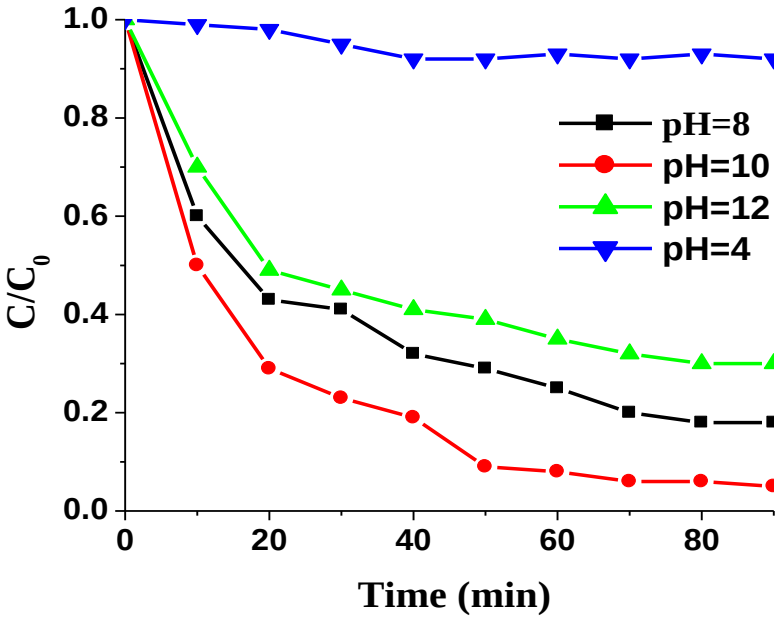

Figure 15. Effect of pH on the degradation of MB by in the presence of Fe_3O_4 NPs (C_0=the initial concentration of MB just immediately after dark equilibrium, C= the concentration of MB at any given time during photocatalysis, t=0 is the time just after 1 h of dark equilibration

Effect of catalyst mass

The photocatalytic degradation of MB under solar irradiation was evaluated at different nanocatalyst masses (10 mg, 20 mg, 30 mg, 40 mg and 50 mg) in 5 mg/L of MB solution. In general, the rate of photocatalytic degradation of MB increases with photocatalyst mass. This is mainly due to increased number of reactive sites and large number hydroxyl radicals produced from irradiated photocatalyst [46, 50-51]. At the lower catalyst loading, degradation of the dye is low since the number of active sites for adsorption is limited, but beyond the optimum amount of catalyst loading, the degradation rate might be reduced due to increase in the opacity of the suspension which causes scattering of light (Figure 16) [51].

The degradation efficiency of 10 mg, 20 mg 30, mg 40 mg and 50 mg of the nanocatalyst after 90 min was 34%, 66%, 94%, 89% and 85% respectively. As a result of this, 30 mg of the nanocatalyst was taken as the optimum mass for 5 mg/L of MB solution.

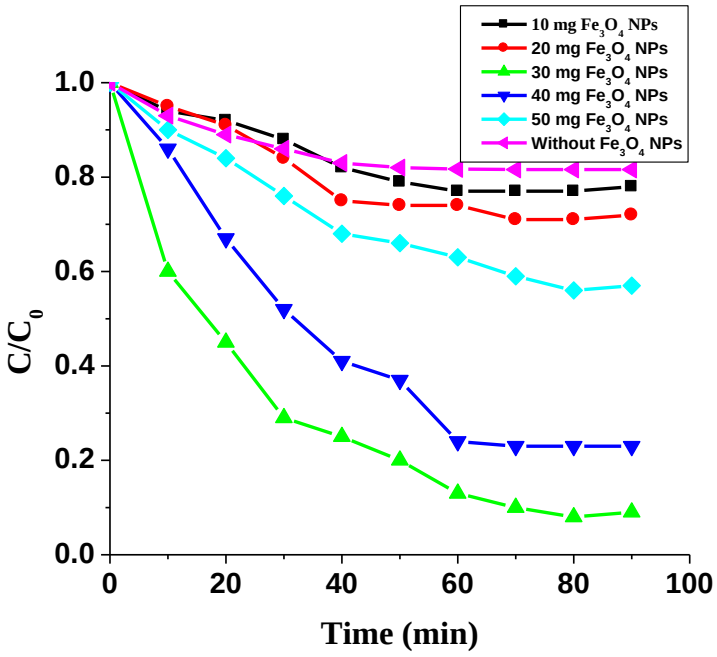

Figure 16. The Effect of catalyst mass on degradation Efficiency of Fe_3O_4 NPs on MB (C_0=the initial concentration of MB just immediately after dark equilibrium, C= the concentration of MB at any given time during photocatalysis, t=0 is the time just after 1h of equilibration

Effect of temperature

The temperature of the photocatalytic reacting system was also studied at 25 ºC, 40 ºC and 60 ºC to explore its effect on the photocatalytic performances of the Fe_3O_4 NPs under visible light irradiation. When the temperature was as high as 60 ºC, the photocatalytic activity was greatly decreased. This is because, high temperature favors the recombination of charge carriers and the enhanced kinetic energy of the dye molecules might allow them to escape from the photocatalyst surface leading to decreased photodegradation efficiency (Figure 17) [50,52-53].

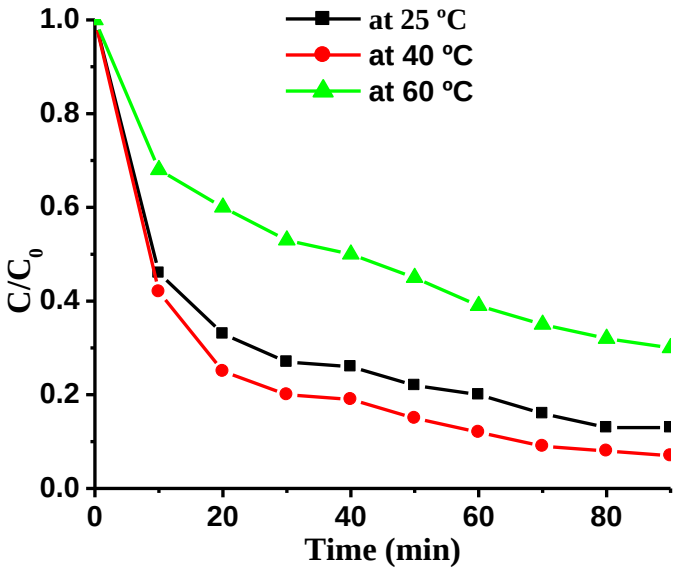

Figure 17. Effect of reaction temperature on photocatalytic degradation of MB by Fe_3O_4 NPs (C_0=the initial concentration of MB just immediately after dark equilibrium, C= the concentration of MB at any time t.

The degradation efficiency of the synthesized Fe_3O_4 NPs after optimizing the parameters (at pH=10.0, mass of Fe_3O_4 NPs=30 mg, concentration of MB=5 mg/L, time of irradiation= 90 min and temperature of the system= 40 ºC) becomes 94.3%.

4.4.3. Reusability of the catalyst

After the reaction has been finished, the catalyst was recovered by a magnet since the synthesized Fe_3O_4 NPs are ferromagnetic and washed with distilled water three times with successive centrifugation at 4500 rpm and dried in an oven for about 7 h. The mass of the recovered catalyst was measured in comparison with originally used 30 mg of the photocatalyst. The recovered amount of the catalyst was used for the next three degradation runs. The recoverability of the photocatalyst (Fe_3O_4 NPs) was 29.7 mg (99% recoverability with 93% degradation efficiency) in the first run, 29.1 mg (97% recoverability with 92.8% degradation efficiency) in the second run and 28.8 mg (96% recoverability with 91% degradation efficiency) in the third run over 1-90 min under visible light irradiation (Figure 18 a and b).

The reusability of the photocatalyst plays a prominent role in the photodegradation process which is a measure of stability of the nanoparticles.

As shown in the indicated figure, the Fe_3O_4 NPs has good photocatalytic activity and the overall decrease in the degradation efficiency of Fe_3O_4 NPs was less than 5%. These results are coherent with previously published literature for the degradation of MB dye using Fe_3O_4 NPs [40]. This insignificant loss of photocatalytic activity indicated the stable structure and reusable nature of the Fe_3O_4 NPs. The slight decrease can be attributed to the loss of photocatalyst between three runs and some refractory intermediates adsorbed on their surface [49-51, 54].

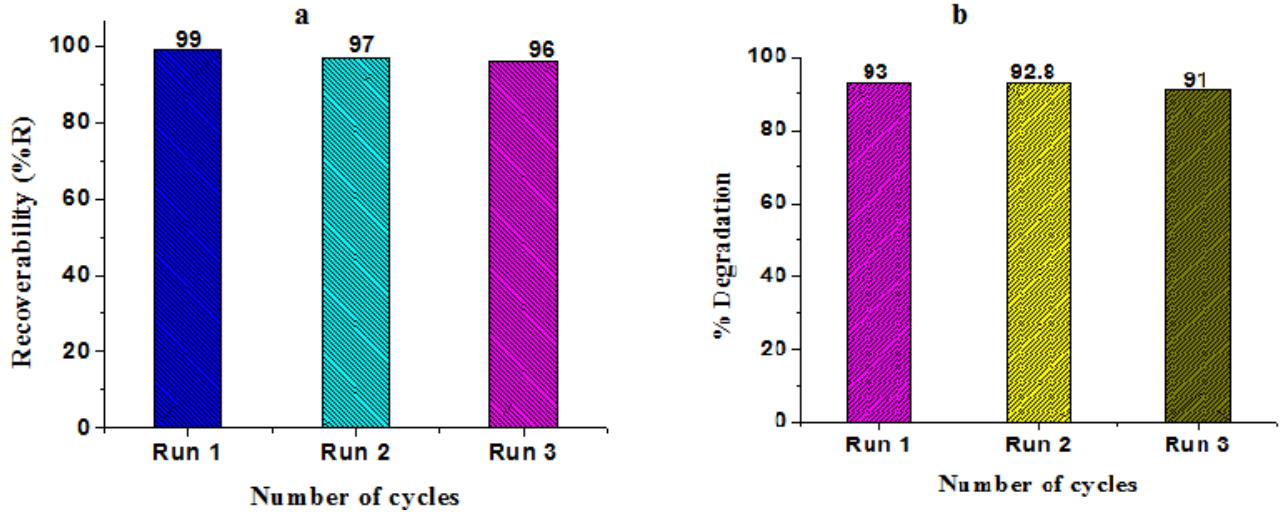

Figure 18. Recoverability (a) and degradation efficiency (b) of Fe_3O_4 NPs photocatalyst in three different runs (initially 30 mg of Fe_3O_4 NPs were used to degrade 5 mg/L of MB solution under solar irradiation)

5. CONCLUSIONS AND RECOMMENDATIONS

5.1. Conclusions

In this study, the Fe_3O_4 NPs were successfully synthesized using an aqueous leaf extract of *Maesa lanceolata* L. as stabilizing agent. The reaction conditions such as temperature, pH, volume of the extract and molar ratio of the precursor iron salts were optimized. The green synthesized Fe_3O_4 NPs show UV-Vis absorption peak at 370 nm. The optical band gap of Fe_3O_4 NPs was determined by Tauc's direct plot method and it is found to be 2.99. This relatively smaller band gap of Fe_3O_4 NPs makes it as selective photocatalyst for model MB degradation. The FT-IR spectroscopy of Fe_3O_4 NPs showed the involvement of functional groups in the synthesis process as stabilizing agent. So, *Maesa lanceolata* L. extract is good stabilizing agent for green synthesis of Fe_3O_4 NPs. The XRD analysis indicates the formation of crystalline Fe_3O_4 NPs with estimated crystalline size to be 14.6 nm, which makes the synthesized nanoparticle a promising candidate for photocatalytic degradation of MB. The findings of this study reveal that the green synthesized Fe_3O_4 NPs showed 94.3% of degradation efficiency after optimizing parameters like initial dye concentration, nanocatalyst mass, pH and temperature of the system to remove MB dye. This significantly high degradation efficiency of Fe_3O_4 NPs is due to their nanomeric size.

5.2. Recommendations

Based on the results obtained from the present study, the following recommendations are made;

- Further characterization techniques like SEM and TEM are needed to determine the shape and particle size of the synthesized Fe_3O_4 NPs.
- Even though, the green synthesized Fe_3O_4 NPs have wide applications, there may be some health related hazards. So it is better if further research studies are conducted in relation to health care.
- Doping with organic or inorganic compounds reduces the optical band gap of nanoparticles to enhance the degradation efficiency of different industrial dye effluents, so that it is advisable if more studies are conducted in synthesis of doped Fe_3O_4 NPs.

REFERENCES

1. Jaafar, B. O.; Hassanain, H.J.; Abdulsalam, M.A. Eco Friendly Synthesis and Characterization of Iron Oxide Nanoparticles by Using Amaranthusspinosus Leaf Extract and Apply It for Domestic Wastewater Treatmen. *J. Research*, **2016**, 3, 9, 65-672.
2. Angela, M.; Gutierreza, T. Dziublaa, Z.H. Recent Advances on Iron Oxide Magnetic Nanoparticles as Sorbents of Organic Pollutants in Water and Wastewater Treatment. *Rev. Environ. Health*. **2017**, 32, 1-2, 111–117.
3. Maas, M.B.; Perold, W.J.; Dicks, L.M. Biosensors for the detection of Escherichia coli, Water. *SA* **2017,** 43.
4. Juan, P.M.; Florentino, L.; Emilio, M.; Oscar, B.; Marciano, S.T.; Alejandra, C.A.; Héctor G.B.; María, L. O.; Alex, G.B.; Verónica, M.R. Synthesis, Characterization, and Sensor Applications of Spinel $ZnCo_2O_4$.*Nanopart., Sens.s.***2016**, 16, 2162,1-14.
5. Tahir, I.; Sunaina, T.; Snobia, G. Synthesis of Silver, Chromium, Manganese, Tin and Iron Nano Particles by Different Techniques. *J. Nanosci. Nanotechnol*. **2017**, 13, 1, 19-52.
6. Makarov, V. V.; Love, A. J.; Sinitsyna, O. V.; Makarova, S. S.; Yaminsky, I. V.; Taliansky, M. E.; N. Kalinina, O. "Green" Nanotechnologies: Synthesis of Metal Nanoparticles Using Plants. *ActA nAturAe*, **2014**, 6, 35-44.
7. Srikanth, N. V.; Sanjay, S. Recent advances and future prospects of iron oxide nanoparticles in biomedicine and diagnostics. *Bio.tech*. **2018,** 8, 279, 1-23.
8. Chemweno, T.; Mwamburi, L.; Korir, R.; Mutuku, A.; Bii C.Antimicrobial Activity and Safety of *Maesa lanceolata* L.for the Treatment and Management of Selected Bacterial Pathogens. *J. Adva. in Microbio.*,**2018,** 8,3, 1-8.
9. Paul, O. O.; Harsh, P. B.; Jorge, M. V.In vitro activities of *Maesa lanceolata* L.extracts against fungal plant pathogens. *Fitoterapia*, **2003,** 312–316.
10. Aman, G.; Narendra, K.J. Advances in green synthesis of nanoparticles. *J. Arti. Cells, Nanomed,, and Biotech*. **2019,** 47:1, 844-851.
11. Balcha, A. Medicinal plants used in traditional medicine in jimma zone, oromia, southwest ethiopia. *Ethiop. J .Health Sci.***2003**, 13, 2, 85-94.
12. Alejandro,L.;América,R.;Enrique, A.;Marco,A.In vitro Antimicrobial Activity Evaluation of Metal Oxide Nanoparticles. **2019,**1-19.

13. Seerangaraj, V.; Selvam, S.;Palanisamy,S.;Felix,L.O.; Arivalagan,P.Biosynthesis of iron oxide nanoparticles using leaf extract of Ruelliatuberosa: Antimicrobial properties and their applications in photocatalytic degradation, *J. Photochem. & Photobio.***2019**, 192,74-82.
14. Ali,T.K.; Muhammad,O.; Ikram, U.; Muhammad, A.; Zabta, K.S.; Malik, M. Biosynthesis of iron oxide (Fe_2O_3) nanoparticles via aqueous extracts of Sageretiathea (Osbeck.) and their pharmacognostic propertie. *Green Chem. Letters and Rev.*, **2017**,10,4, 186-201.
15. Subha, V.; Divya, K.; Gayathri, S.; Jagan, M.E.; Keerthanaa, N.; Vinitha, M.; Kirubanandan, S.; Renganathan, S. Applications of iron oxide nano composite in waste water treatment–dye decolourisation and anti– microbial activity. *MO. J. Drug Desi. Develop. & Thera.* **2018**, 2,5, 178-184.
16. Sadia, S.; Arifa, T.; Yongsheng, C. Green Synthesis of Iron Nanoparticles and Their Environmental Applications and Implications. *Nanomater.* **2016**,6,209,1-26.
17. Shaan, B.J. Khuram, S. A. Foliar-mediated Ag:ZnO nanophotocatalysts: green synthesis, characterization, pollutants degradation, and in vitro biocidal *activity. Green Proc. Synth.***2019**, 8, 172–182.
18. Haijiao,L.;Jingkang,W.; Marco,S.;Ting,W.; Ying,B.;Hongxun,H. An Overview of Nanomaterials for Water and Wastewater Treatment. *Hind. Publi. Corpo.***2016,** 5, 1-11.
19. Eunice, A.; Denise, V.; José, I.S.; Elizabeth, R.)' Synthesis, Characterization and Applications of Iron Oxide Nanoparticles – a Short Review**.** *J. Aerosp. Technol. Manag., São José dos Campos*, **2015,** 7, 3, 267-276.
20. KATJA, A. S.*Essentials of Inorganic Chemistry*.School of Pharmacy, University of Reading, UK J. Wiley & Sons, Ltd,**2015**.
21. Attarad A.Z.; Muhammad, Z.; Ihsan, H.; Abdul, R.P.; Joham ,S. A.;Altaf, H. Synthesis, characterization, applications, and challenges of iron oxide nanoparticles. *Nanotech. Sci.and Appli.***2016**, 9,49-67.
22. Shabnam, F.; Mina, J.; Hassan, K.F. Green synthesis of zinc oxide nanoparticles' *a comparison. J.green Chem. Letters and Rev.* **2019**, 12, 1, 19-24.
23. Dhermendra, K.; Behari, J.; Prasenjit, S. Application of Nanoparticles in Waste Water Treatment' *World App. Sci. J.*, **2008**, 3, 3, 417-433.

24. Ajey Singha, N. B. Singha.; Imtiyaz, H.; Himani, S.; S.C. Singhb. Plant-nanoparticle interaction: An approach to improve agricultural practices and plant productivity. *J. Pharm.Sci. In.***2015**, 4, 8,25-40.

25. Ian, S. Y.; Harwin, A. K.; Dendy, A.; Antonius, I. Nanotechnologies in water and air pollution treatment, *Env. Techno. Reviews.* **2012**, 1, 1, 136-148.
26. Atul, M. K.; Anjna, S.; Indresh, K. M.; Alpana, T.; Sunil, K. Synthesis of ultra-small iron oxide and doped iron oxide nanostructures and their antimicrobial activities, *J. of Taibah Uni. for Sci*, **2019**,13,1, 280-285.
27. Mohammed, M. R.; Sher, B. K.; Aslam, J.; Mohd, F.;Abdullah, M. A. Iron Oxide Nanoparticles.**2014,**1-25.
28. Khwaja, S.; Aziz, R.; Tajuddin, Azamal, H. Biogenic Fabrication of Iron/Iron Oxide Nanoparticles and Their Application. *Nanoscale Rese. Lett.* **2016,** 11, 498.
29. Alper, K.; Bekir, K. General Evaluations of Nanoparticles. *El-Cezerî J. of Sci. and Eng.* **2018**, 5, 1, 191-236.
30. El-Shal,A.M.; Shereen, M. A. and Hassan, A. M. H. A facile nano-iron oxide sensor for the electrochemical detection of the antidiabetic drug linagliptin in the presence of glucose and metformin. *Bulletin of the Nat. Rese. Centre,* **2019,** 1- 8.
31. Pandey G. A review on the factors affecting the photocatalytic degradation of hazardous materials. *Material Sci & Eng Int J.* **2017,** 1, 3,106–114.
32. Ali, S.; Seyed, A.H. ; Hossein, I.; Nastaran, K. Purification of Methylene Blue via Photocatalytic Nanofibrous Membranes Containing TiO_2 Nanoparticles. *J. of Engi. Fib. and Fab*.**2016,** 11,4,43-55.
33. Ghassan, M. S.; Amer, T. T.; Amal, S. N. Biosynthesis, characterization of magnetic iron oxide nanoparticles and evaluations of the cytotoxicity and DNA damage of human breast carcinoma cell lines, *Arti. Cells, Nanomed. and Biotech.***2018,** 46,6, 1215-122.
34. Laurent,S.; Boutry, S.;Muller,R.N. Metal oxide particles and their prospects for application. *Elsevier Ltd*. **2018**.1-40.
35. Nigus, A.S.; Lijalem, H.A.; Leta, D.T. Chemical composition and antimicrobial activity of leaf extract of Ocimum lamiifolium (Damakese) as a treatment for urinary tract infection. *Cogent Chem.***2018**, 4: 1-10.

36. Marziyah, S.;Hasse, H.;Mohammed, H.Experimental study of influencing factors and kinetics in catalytic removal of Methylene Blue with TiO_2 nanopowder. *Amer.J. of Env. Engi*.**2012**, 2, 1, 1-7.
37. Shahana, B.; Aarti, K.; Raja, S. Facile synthesis of magnetic iron oxide nanoparticles using inedible *Cynometra ramiflora* fruit extract waste and their photocatalytic degradation of methylene blue dye. *Mat. Res. Bul.* **2018**, 97, 121–127.
38. Tsegaye, G.A.; Gijs, D.L. Zn-doped CdSe nanoparticles: Impact of synthesis conditions on photocatalytic activity. *Env.Tech.& Inno.***2020**,20,1-13.
39. Hassanien, A.S.; Aly, K.A.; Akl, A.A. Study of optical properties of thermally evaporated ZnSe thin films annealed at different pulsed laser powers, *J. of Al.s and Comp.* **2016,** 06,180, 1-38.
40. Monika, G.; Rajesh, S. T.; Shuchi, K.; Raghvendra, K. M.; Divakar, S. Effective Antimicrobial Activity of Green ZnO Nano Particles of Catharanthus roseus. *Front. Microbiol.* **2018**,9,1-13.
41. Nimali, N. P. Green synthesis of iron oxide nanoparticles (IONPs) and their nanotechnological applications. *J. Bacter. Mycol. Open Access.* **2018,** 6, 4, 260–262.
42. Rajasekhar, C.; Gan, G. R. Green Synthesis of Metal Nanoparticles and its Reaction Mechanism. *Scri. Pub. LLC*.**2018**, 113–139.
43. Yen, P. Y.; Kamyar, S.; Mikio, M.; Noriyuki, K.; Nurul, B.; Bt Ahmad, K. S.; Kar X. L. Green Synthesis of Magnetite (Fe_3O_4) Nanoparticles Using Seaweed (Kappaphycus alvarezii) Extrac. *Nano. Res. L.* **2016,** 11,276,1-7.
44. Nayereh, S.; Elias, S.; Mohd, Z.H.; Maryam, E. Alam, A.; Ghazaleh, B.; Manizheh, N.; Parisa, V. Visible Light-Induced Degradation of Methylene Blue in the Presence of Photocatalytic ZnS and CdS Nanoparticles. *J. Mol. Sci.* **2012**, *13*, 12242-12258.
45. Ramesh, A. V.; Dharmasoth, R. D.; Satish, M. B.; Basavaiah. K. Facile green synthesis of Fe_3O_4 nanoparticles using aqueous leaf extract of Zanthoxylum armatum DC. for efficient adsorption of methylene blue. *J. of Asian Cera. Soci.* **2018,** 6, 2, 145-155.
46. Tamrat, T.A.; A Review on Traditionally Used Medicinal Plants/Herbs for Cancer Therapy in Ethiopia: Current Status, Challenge and Future Perspectives. *Organic Chem. Curr. Res.* **2018**, 7,2,1-8.

47. Amutha, S.; Sridhar, S. Green synthesis of magnetic iron oxide nanoparticle using leaf of Glycosmis mauritiana and their antibacterial activity against human pathogens. *J. of Inno. in Pharm. and Bio. Sci.* **2018,** 5, 2, 22-26.
48. Hassena, H.; Photocatalytic Degradation of Methylene Blue by Using Al_2O_3/Fe_2O_3 Nano Composite under Visible Light. *Mod. Chem. Appl.* **2016,** 4: 176,1-5.
49. Gnanaprakasam,A.; Sivakumar, V.M.; Thirumarimurugan, M. Influencing Parameters in the Photocatalytic Degradation of Organic Effluent *via* Nanometal Oxide Catalyst: A Review. *Indian J. of Mater. Sci.* **2015**, 1-16.
50. Hesham, F.; Aly1, A.;Ibrahim, A. Photocatalytic Degradation of Methylene Blue Dye Using Silica Oxide Nanoparticles as a Catalyst. WATER ENV. RES. **2018**, 806-818.
51. Suhila, A.;Aicha, M.;Elbashir, E.;Ali, S. Photocatalytic degradation of mrthylene blue dye in aqueous solution by $MnTiO_3$ nanoparticles under sun light irradiation. *Cell pre.Heli.***2020**,6,1-6.
52. Sunitha, M.; Sekhar, R. S.; Ravali, B.; Reddy, R. K.; Mahalakshmi1, S.V.; Sruthi1, V.; Paul D.S. Visible Light Photocatalytic Degradation of Methylene Blue and Malachite Green Dyes with $BaWO_4$-Go Nano Composite**.** *J. Envi., Agri. and Biotech.***2017,** 2,3, 1173-1183.
53. Sandhya, J.; Kalaiselvam, S. Biogenic synthesis of magnetic iron oxide nanoparticles using inedible borassus flabellifer seed coat: characterization, antimicrobial, antioxidant activity and in vitro cytotoxicity analysis. *Mater. Res. Express.***2020,** 7, 1-15.
54. SARANYA, S.; VIJAYARANI, K.; PAVITHRA, S. Green Synthesis of Iron Nanoparticles using Aqueous Extract of *Musa ornata* Flower Sheath against Pathogenic Bacteria. *Indian J. of Phar. Sci.* **2017,**79,5, 688-694.

APPENDICES

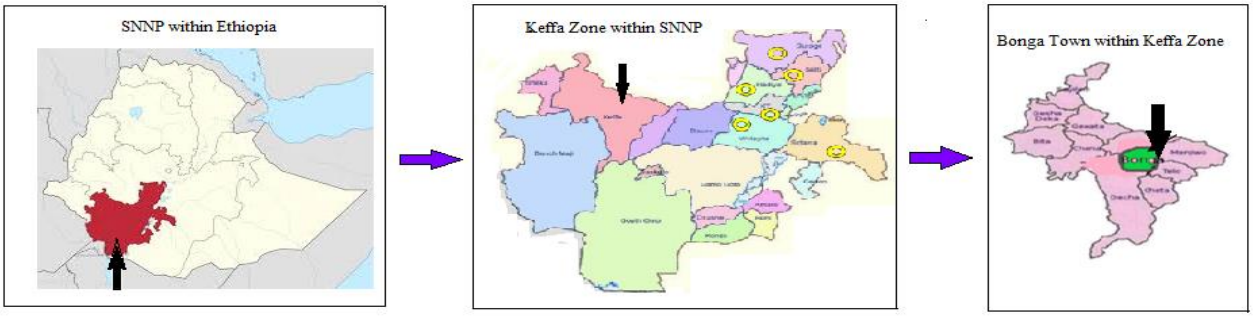

Appendix 1. Map of the plant samples collection area (taken from the Kaffa Zone Administration Office)

Appendix 2. *Maesa lanceolata* L. / / (photo taken from local garden near Bonga University)

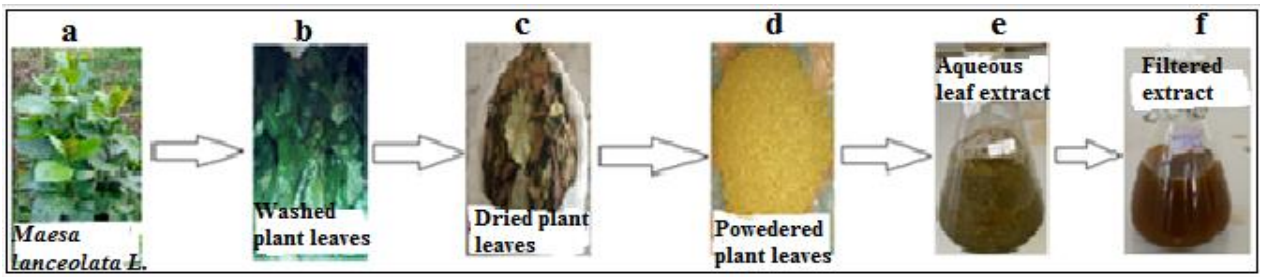

Appendix 3. Schematic representation of Extraction of *Maesa lanceolata L*. leaf

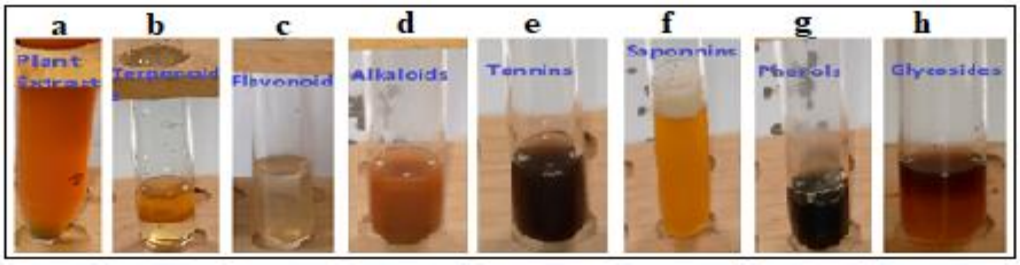

Appendix 4. Phytochemical screening test of crude aqueous leaf extract of *Maesa lanceolata* L.

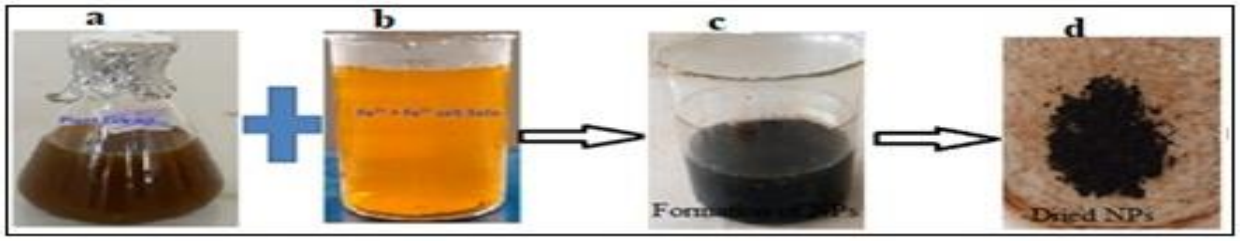

Appendix 5. Synthesis steps of Fe_3O_4 NPs

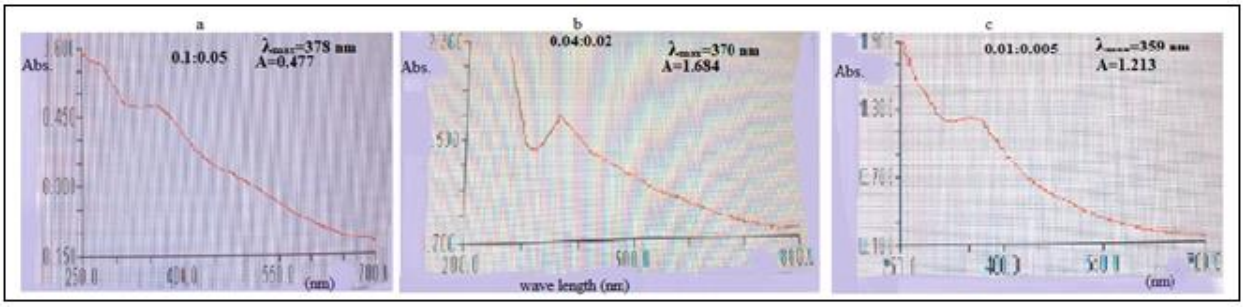

Appendix 6. The effect of the ratio of concentration of $FeCl_3.6H_2O$ to $FeCl_2.4H_2O$ for the green synthesis of Fe_3O_4 NPs

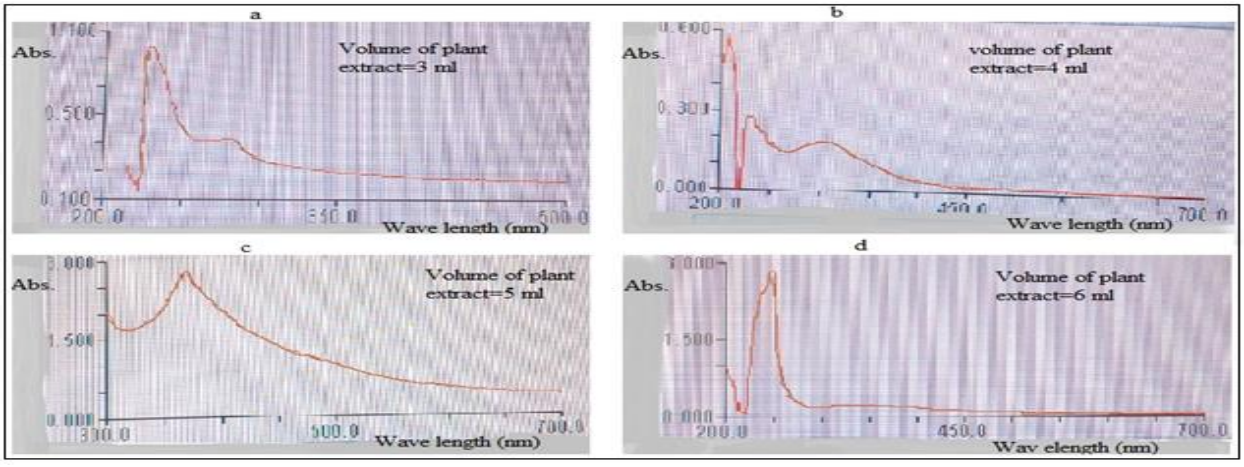

Appendix 7. The effect of the volume of the plant extract for the green synthesis of Fe_3O_4 NPs

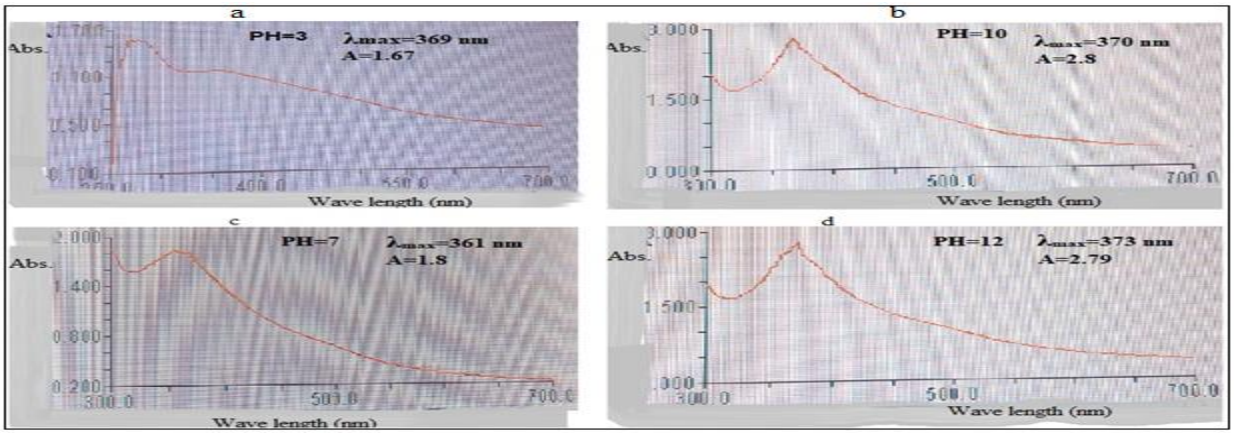

Appendix 8. The effect of the PH of the solution for the green synthesis of Fe_3O_4 NPs

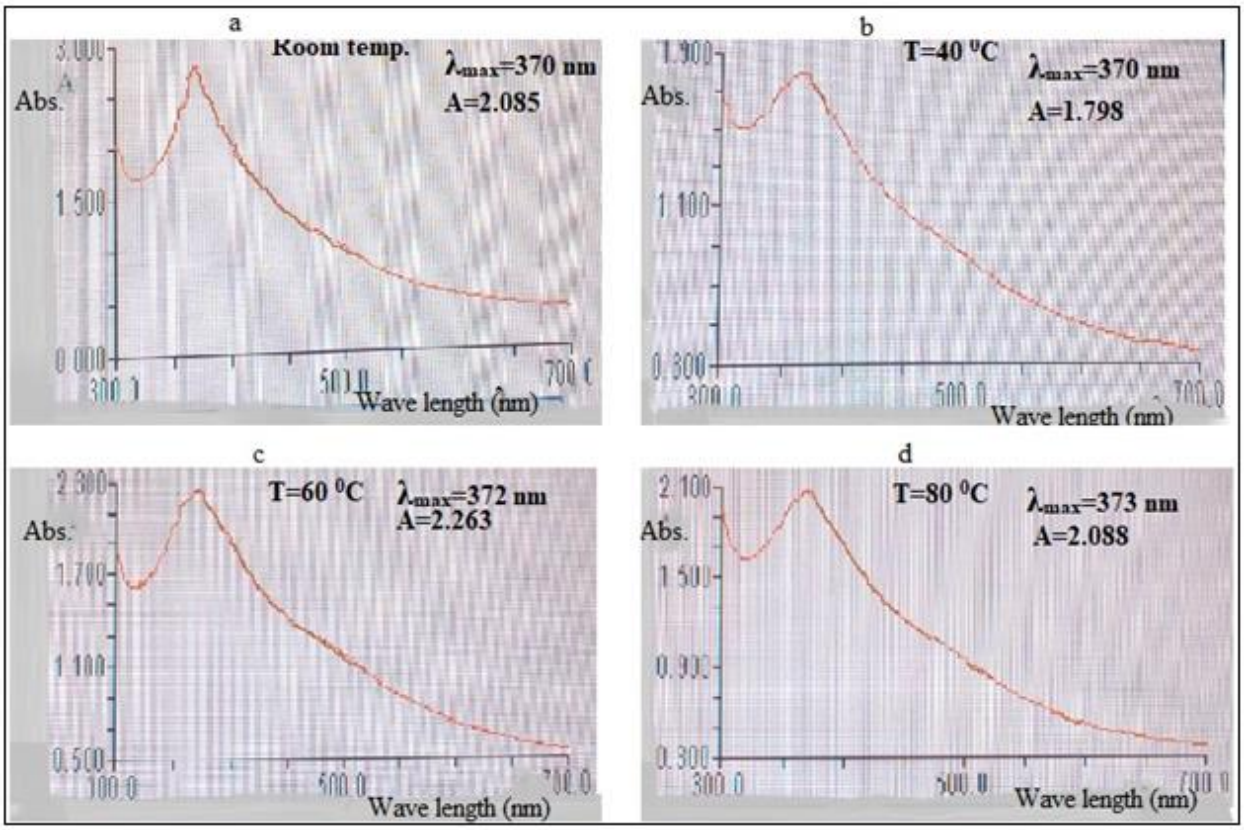

Appendix 9. The effect of temperature for the green synthesis of Fe_3O_4 NPs

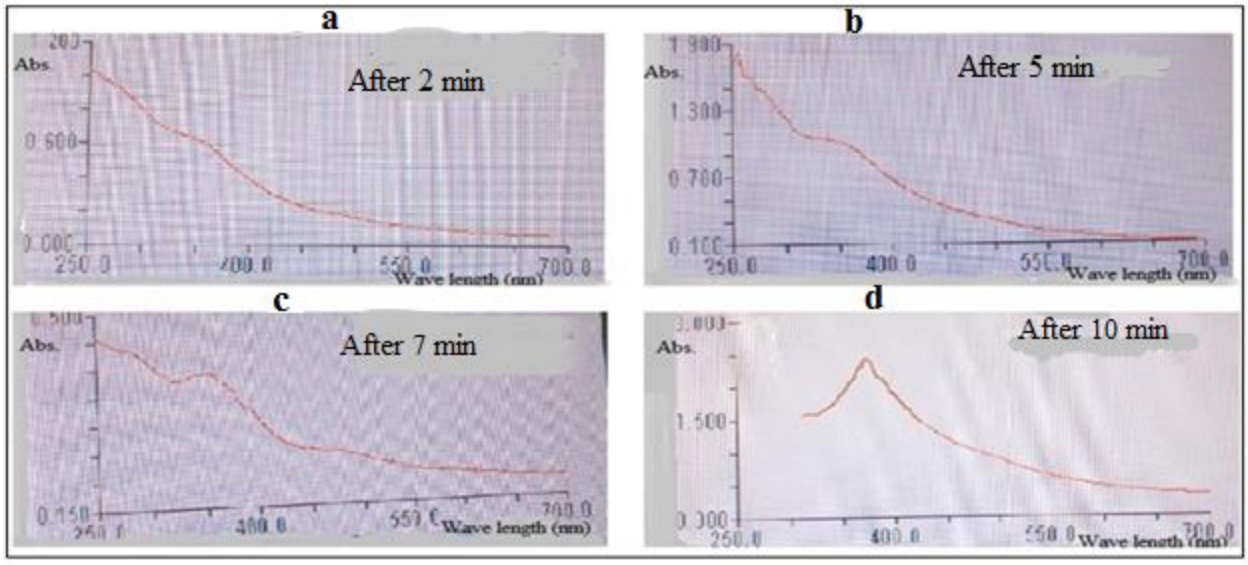

Appendix 10. The effect of the reaction time for the green synthesis of Fe_3O_4 NP.

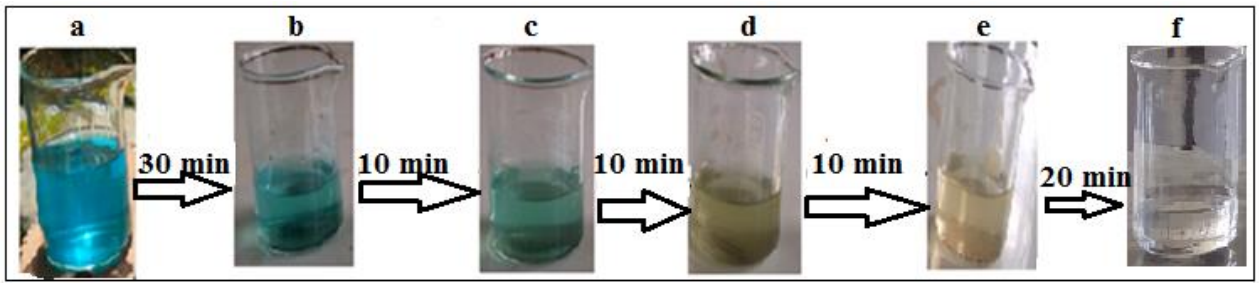

Appendix 11. Schematic representation of the photocatalytic degradation of 5 mg/L MB solution with time factor in the presence of 30 mg of Fe_3O_4 NPs

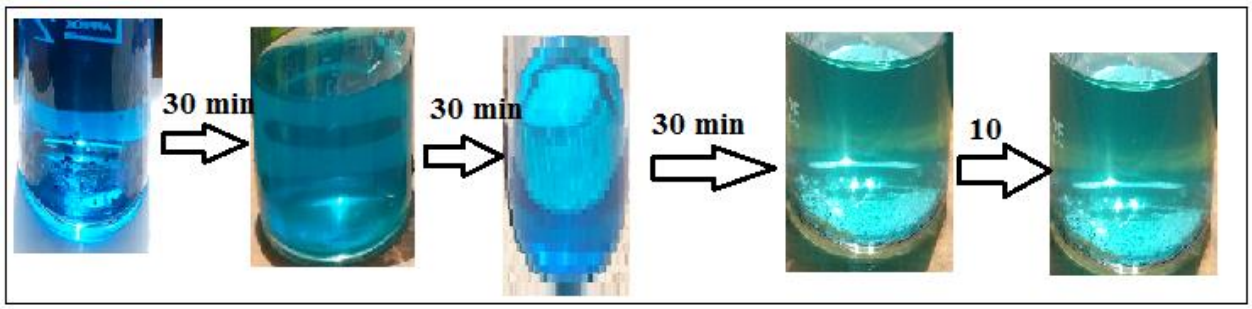

Appendix 12. Schematic representation of the photolysis of 5 mg/L MB solution with time factor in the absence of 30 mg of Fe_3O_4 NPs